Sustainable Cities and Society 117 (2024) 105928

Contents lists available at ScienceDirect

Sustainable Cities and Society

journal homepage: www.elsevier.com/locate/scs

Operational sensitivity analysis of flooding volume in urban areas

Leonardo Sandoval, Aronne Dell'Oca, Monica Riva *

Dipartimento di Ingegneria Civile e Ambientale, Politecnico di Milano, Piazza L. Da Vinci 32, Milan, 20133, Italy

ARTICLE INFO

Dataset link: https://zenodo.org/records/13742805

Keywords:
Global sensitivity analysis
Urban flooding
Operational interventions
Uncertainty
Probability of system failure

ABSTRACT

We focus on a probability-based approach to analyze the flooding volume during extreme rainfall events in urban areas. Our approach considers uncertainty in both *non-operational* and *operational* variables. The former are quantities that are tied to the characterization of rainfall events and key catchment features, whose uncertainties stem from incomplete characterization. The latter comprise elements of the system on which actions can be taken within a range of design values. As the non-deterministic nature of these two types of quantities differs at a fundamental level, we rely on an operational Global Sensitivity Analysis theoretical framework that explicitly recognizes this distinction. As a test bed to showcase our approach, we consider an urban catchment in Northern Italy. We assess the sensitivity of the flooding volume to a set of *operational* variables, such as diameter and roughness of a set of conduits of the sewer network as well as potential improvement of the infiltration capacity of the urban catchment. We show that our approach can identify the operational configuration with the highest effectiveness in mitigating instances of flooding, taking into account the uncertainties in the *non-operational* quantities that drive the system behavior.

1. Introduction

The sustainable development of urban communities is strongly influenced by their ability to cope with intense rainfall events. The increased severity of these events, as related to global changes, along with the increased degree of urbanization underpins the documented intensification of flooding in urban areas (Gray, Zhao, & Stillwell, 2023; KC, Shrestha, Ninsawat, & Chonwattana, 2021; Li et al., 2021; Liu et al., 2020; Mahmoud & Gan, 2018; Satterthwaite, 2008; Semadeni-Davies, Hernebring, Svensson, & Gustafsson, 2008; Tellman et al., 2021; Yin et al., 2018). These scenarios are also associated with diverse economic, health, environmental, and safety issues (Bhuiyan, Er, Muhamad, & Pereira, 2022; Chauhan, Dongol, & Chauhan, 2023; Hammond, Chen, Djordjević, Butler, & Mark, 2015; Jato-Espino, Toro-Huertas, & Güereca, 2022; de Macedo et al., 2023; Mobini, Pirzamanbein, Berndtsson, & Larsson, 2022; ten Veldhuis, 2011).

A key challenge for stormwater management is related to the capability of an urban system to effectively cope with large volumes of water that can be conveyed through the sewer system without resulting in system failure and subsequent flooding events (Arnbjerg-Nielsen et al., 2013; Ashley, Balmforth, Saul, & Blanskby, 2005; Azari & Tabesh, 2022; D'Ambrosio & Longobardi, 2023; Haghighatafshar et al., 2020; Hesarkazzazi et al., 2022). This challenge is often exacerbated by the omnipresent uncertainty associated with rainfall-runoff processes (da Silva, Alencar, & de Almeida, 2022; Dell'Oca, Guadagnini, & Riva, 2023; Dong, Yu, Farahmand, & Mostafavi, 2020; Iradukunda, Mwanaumo, & Kabika, 2023; KC et al., 2021; Pour, Wahab, Shahid, Asaduzzaman, & Dewan, 2020; Suresh, Pekkat, & Subbiah, 2023; Wang et al., 2023; Wang, Zhang, Chen, Wang and Fu, 2023; Xu, Zhong, Chen, & Zhang, 2023). Uncertainties related to our understanding of the dynamics of urban runoff generation arise from our incomplete knowledge about (*i*) characteristics of future rainfall events (Forsee & Ahmad, 2011; Gray et al., 2023; Huong & Pathirana, 2013; Jung, Chang, & Moradkhani, 2011; Liu et al., 2023; O'Donnell & Thorne, 2020; Pińskwar, Choryński, & Graczyk, 2023) and (*ii*) properties driving the hydrological and hydraulic behavior of the catchment and sewer system, respectively (Huong & Pathirana, 2013; Ju et al., 2023; Jung et al., 2011; Miller & Hutchins, 2017).

The presence of these sources of uncertainty has favored the use of probabilistic approaches to assess urban flooding events and to design ensuing engineering solutions (Bodoque, Esteban-Muñoz, & Ballesteros-Cánovas, 2023; Haghighatafshar et al., 2020; Hu et al., 2021; Liu et al., 2023; Piyumi, Abenayake, Jayasinghe, & Wijegunarathna, 2021; Zhao, Gu, Tang, Gong, & Zhao, 2023). In this context, Jung et al. (2011) investigate the relevance of uncertainties related to climate change, land use, and hydrological parameters on urban flooding. Tavakol-Davani et al. (2016) assess the benefits of rainwater harvesting interventions in reducing sewer overflow under climate change scenarios. Mahaut and Andrieu (2019) evaluate the impact of diverse urban developments

* Corresponding author.
E-mail address: monica.riva@polimi.it (M. Riva).

https://doi.org/10.1016/j.scs.2024.105928
Received 29 May 2024; Received in revised form 26 September 2024; Accepted 20 October 2024
Available online 2 November 2024

and water management approaches on sewer system overflows upon considering various scenarios of climate change. Hu et al. (2021) highlight the relevance of considering alternative model formulations of the rainfall-runoff process on the reliability of flooding predictions. Suresh et al. (2023) quantify the efficiency of low-impact developments in mitigating flooding in urban areas. Zhao et al. (2023) highlight the benefits of pursuing sustainable land cover development in urban areas to cope with the exacerbation of rainfall events. Liu et al. (2023) document an increase of more than 50% in the probability of flooding in Beijing (China) when considering diverse possible climate scenarios.

This series of studies highlights the need for considering multiple sources of uncertainty associated with diverse and interconnected hydrological factors when evaluating alternative engineering actions that can be implemented to enhance the current capability of an urban drainage system. In this context, global sensitivity analysis (GSA) serves as a valuable tool to quantify the impact of uncertainties on the efficiency of urban drainage systems. Uncertainties can be related to variables on which one cannot intervene, such as the intensity or duration of a rain event (hereafter denoted as *non-operational* variables) as well as with elements of the system on which we can intervene and for which we can engineer a plausible range of design values, such as the diameter of a pipe in a sewer system (hereafter denoted as *operational* variables). While the nature of variability in the *non-operational* and *operational* variables is markedly different, classical GSA approaches do not recognize this aspect (Pianosi et al., 2016; Razavi et al., 2021). A recent methodological framework, termed operational sensitivity analysis (SA) has been proposed by Dell'Oca (2023) to overcome this limitation. Operational SA quantifies the sensitivity of a model quantity of interest to *operational* variables whilst considering the uncertainty in the *non-operational* variables. In other words, while classical GSA addresses the question 'What is the relevance of the uncertain (i.e., *operational* and *non-operational*) variables on a quantity of interest?', operational SA addresses the question 'What is the relevance of the diverse *operational* variables (upon which one could intervene), given the uncertainty in the *non-operational* variables?'

The present work focuses on a scenario of urban flooding where the actual sewer system is unable to cope with stormwater during extreme events. In such a system, we identify a set of *non-operational* variables (that includes uncertain hydrological properties of the urban area and characteristics of the rainfall event) and *operational* variables (which are related to the properties of a set of sewer pipes and the infiltration capacity of the urban area). First, we rely on traditional GSA metrics to assess the sensitivity of the flooding volume to *non-operational* variables, while keeping the *operational* variables at their current design values. We then resort to operational SA metrics to quantify the sensitivity of the flooding volume to the *operational* variables, thus providing guidance for designing future interventions on the system.

2. Methodology and materials

This Section is devoted to introducing (i) the GSA metrics considered to quantify the sensitivity of a model output of interest with respect to a system/model variable; (ii) the modeling approach adopted in this study to represent a given hydraulic-hydrological urban system; and (iii) an overview of the study area where we showcase our approach.

2.1. Moment- and probability-based GSA

Here, we briefly recall the theoretical foundations and definitions of the moment- (Dell'Oca, Riva, & Guadagnini, 2017) and probability-based (la Cecilia, Porta, Tang, Riva, & Maggi, 2020) global sensitivity indices employed in this study. Considering a model whose output y is a function of a collection of random variables (collected in vector $\boldsymbol{\eta}$), the mean and the (centered) n-order statistical moment of y (with, e.g., $n = 2$ or 3 for the variance or skewness, respectively) are defined as

$$E^y_{\boldsymbol{\eta}} = \int_{\Gamma_{\boldsymbol{\eta}}} y(\boldsymbol{\eta}) p_{\boldsymbol{\eta}} d\boldsymbol{\eta}, \quad (1)$$

$$SM^{y,(n)}_{\boldsymbol{\eta}} = \int_{\Gamma_{\boldsymbol{\eta}}} \left\{ y(\boldsymbol{\eta}) - E^y_{\boldsymbol{\eta}} \right\}^n p_{\boldsymbol{\eta}} d\boldsymbol{\eta}, \quad (2)$$

where $\Gamma_{\boldsymbol{\eta}}$ and $p_{\boldsymbol{\eta}}$ denote the support and the probability density function (pdf) of $\boldsymbol{\eta}$, respectively. The mean and n-order statistical moment of y conditional to the uncertain model variable η_i can be evaluated as

$$E^y_{\sim\eta_i} = \int_{\Gamma_{\sim\eta_i}} y(\boldsymbol{\eta}) p_{\sim\eta_i} d\boldsymbol{\eta}_{\sim\eta_i}, \quad (3)$$

$$SM^{y,(n)}_{\sim\eta_i} = \int_{\Gamma_{\sim\eta_i}} \left\{ y(\boldsymbol{\eta}) - E^y_{\sim\eta_i} \right\}^n p_{\sim\eta_i} d\boldsymbol{\eta}_{\sim\eta_i}, \quad (4)$$

where $\Gamma_{\sim\eta_i}$ is the space of all entries of $\boldsymbol{\eta}$ excluding η_i, $p_{\sim\eta_i}$ being the corresponding pdf. Following Dell'Oca et al. (2017), the sensitivity of the mean of y to η_i can be assessed by the following index

$$\mathrm{AMA}E_{\eta_i} = \int_{\Gamma_{\eta_i}} \left| E^y_{\boldsymbol{\eta}} - E^y_{\sim\eta_i} \right| p_{\eta_i} d\eta_i. \quad (5)$$

In a similar way, the sensitivity of the n-order statistical moment of y to η_i can be evaluated through

$$\mathrm{AMA}SM^{(n)}_{\eta_i} = \int_{\Gamma_{\eta_i}} \left| SM^{y,(n)}_{\boldsymbol{\eta}} - SM^{y,(n)}_{\sim\eta_i} \right| p_{\eta_i} d\eta_i. \quad (6)$$

The set of indices in Eqs. (5)–(6) quantify the sensitivity of y to η_i as the (average) degree of variability in a given statistical moment of y that is ascribable to variations of η_i. The joint inspection of indices in Eqs. (5)–(6) allows for a comprehensive assessment of the impact of variable η_i on the model output y. A high value of $\mathrm{AMA}E_{\eta_i}$ or $\mathrm{AMA}SM^{(n)}_{\eta_i}$ indicates a strong influence of η_i on the mean value or on the n-order statistical moment of y, respectively (see also Dell'Oca et al., 2017). As an example, Fig. 1 illustrates the workflow for evaluating $\mathrm{AMA}E_{\eta_i}$ when the model output y depends on three variables, i.e. $\boldsymbol{\eta} = (\eta_1; \eta_2; \eta_3)$. These are sampled by drawing an ensemble of random realizations of $\boldsymbol{\eta}$ upon which $y(\boldsymbol{\eta})$, $E^y_{\boldsymbol{\eta}}$, and $E^y_{\sim\eta_i}$ are evaluated. Then, Eq. (5) is applied to compute $\mathrm{AMA}E_{\eta_i}$. The same strategy is implemented to evaluate $\mathrm{AMA}SM^{(n)}_{\eta_i}$ in Eq. (6).

Following la Cecilia et al. (2020), we introduce the global sensitivity index that quantifies the sensitivity of the probability of y to exceed a threshold k (i.e., the exceedance probability $P^y_{\boldsymbol{\eta}}(k) = Pr(y(\boldsymbol{\eta}) \geq k)$ with respect to the variability of η_i as

$$\mathrm{AMA}P_{\eta_i} = \int_{\Gamma_{\eta_i}} \left| P^y_{\boldsymbol{\eta}}(k) - P^y_{\sim\eta_i}(k) \right| p_{\eta_i} d\eta_i, \quad (7)$$

where $P^y_{\sim\eta_i}(k)$ is the exceedance probability conditional to η_i, i.e., $P^y_{\sim\eta_i}(k) = Pr(y(\boldsymbol{\eta}) \geq k|\eta_i)$. The $\mathrm{AMA}P_{\eta_i}$ index ranges from 0 to 1 and quantifies the sensitivity of y to η_i as the (average) variability in the exceedance probability of y resulting from changes in η_i. High values of $\mathrm{AMA}P_{\eta_i}$ indicate that the exceedance probability is clearly impacted by η_i, i.e. η_i should be factored into policies aimed at reducing the risk of system failure (see also la Cecilia et al., 2020).

2.2. Non-operational and operational system variables

Dell'Oca (2023) emphasize the distinct nature of the random variables collected in $\boldsymbol{\eta}$ by distinguishing in *non-operational*, $\boldsymbol{\omega}$, and *operational*, $\boldsymbol{\theta}$, variables, i.e., $\boldsymbol{\eta} = (\boldsymbol{\omega}, \boldsymbol{\theta})$. In particular, quantities included in $\boldsymbol{\omega}$ typically encompass environmental quantities over which we have minimal (or no) control. The degree of variability associated with $\boldsymbol{\omega}$ corresponds to our limited knowledge of the system. For instance, within the realm of hydraulic-hydrological engineering scenarios, rainfall intensity can be considered a *non-operational* random variable. On the other hand, quantities included in $\boldsymbol{\theta}$ are *operational* (or design) factors that we can modify and manage. The degree of variability assigned to $\boldsymbol{\theta}$ reflects the ranges of *operational* (or design) values one

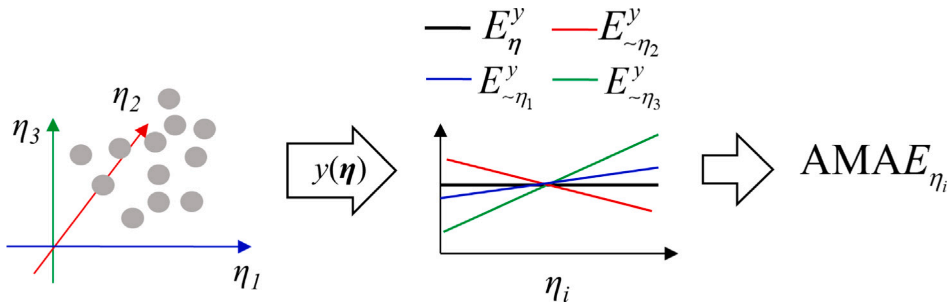

Fig. 1. Workflow for the evaluation of AMAE_{η_i}. (For interpretation of the references to color in this figure legend, the reader is referred to the web version of this article.)

takes into account when designing interventions or modifications of the system. For instance, the diameter of a sewer pipe can be considered a random *operational* variable when designing hydraulic engineering actions in urban areas.

Under these premises, a model output is a function of both *operational* and *non-operational* variables, i.e., $y = y(\boldsymbol{\eta}) = y(\boldsymbol{\omega}, \boldsymbol{\theta})$. Therefore, we can introduce the expected value of y with respect to $\boldsymbol{\omega}$, and $\boldsymbol{\theta}$ as

$$E^y_{\boldsymbol{\theta}}(\boldsymbol{\omega}) = \int_{\Gamma_{\boldsymbol{\theta}}} y(\boldsymbol{\omega}, \boldsymbol{\theta}) p_{\boldsymbol{\theta}} d\boldsymbol{\theta}; \qquad E^y_{\boldsymbol{\omega}}(\boldsymbol{\theta}) = \int_{\Gamma_{\boldsymbol{\omega}}} y(\boldsymbol{\omega}, \boldsymbol{\theta}) p_{\boldsymbol{\omega}} d\boldsymbol{\omega}. \tag{8}$$

Note that $E^y_{\boldsymbol{\theta}}(\boldsymbol{\omega})$ and $E^y_{\boldsymbol{\omega}}(\boldsymbol{\theta})$ are random quantities due to the randomness in $\boldsymbol{\omega}$ and $\boldsymbol{\theta}$, respectively. In a similar way, one can define nth order centered statistical moment of y, i.e.,

$$SM^{y,(n)}_{\boldsymbol{\theta}}(\boldsymbol{\omega}) = \int_{\Gamma_{\boldsymbol{\theta}}} \left\{ y(\boldsymbol{\omega}, \boldsymbol{\theta}) - E^y_{\boldsymbol{\theta}}(\boldsymbol{\omega}) \right\}^n p_{\boldsymbol{\theta}} d\boldsymbol{\theta}, \tag{9}$$

$$SM^{y,(n)}_{\boldsymbol{\omega}}(\boldsymbol{\theta}) = \int_{\Gamma_{\boldsymbol{\omega}}} \left\{ y(\boldsymbol{\omega}, \boldsymbol{\theta}) - E^y_{\boldsymbol{\omega}}(\boldsymbol{\theta}) \right\}^n p_{\boldsymbol{\omega}} d\boldsymbol{\omega}, \tag{10}$$

where both $SM^{y,(n)}_{\boldsymbol{\theta}}(\boldsymbol{\omega})$ and $SM^{y,(n)}_{\boldsymbol{\omega}}(\boldsymbol{\theta})$ are random quantities. For completeness, we also introduce the mean and n-order statistical moments conditional to ω_i,

$$E^y_{\sim\omega_i}(\boldsymbol{\theta}) = \int_{\Gamma_{\sim\omega_i}} y(\boldsymbol{\omega}, \boldsymbol{\theta}) p_{\sim\omega_i} d\boldsymbol{\omega}_{\sim\omega_i}, \tag{11}$$

$$SM^{y,(n)}_{\sim\omega_i}(\boldsymbol{\theta}) = \int_{\Gamma_{\sim\omega_i}} \left\{ y(\boldsymbol{\omega}, \boldsymbol{\theta}) - E^y_{\sim\omega_i}(\boldsymbol{\theta}) \right\}^n p_{\sim\omega_i} d\boldsymbol{\omega}_{\sim\omega_i}, \tag{12}$$

and to θ_i,

$$E^y_{\sim\theta_i}(\boldsymbol{\omega}) = \int_{\Gamma_{\sim\theta_i}} y(\boldsymbol{\omega}, \boldsymbol{\theta}) p_{\sim\theta_i} d\boldsymbol{\theta}_{\sim\theta_i}, \tag{13}$$

$$SM^{y,(n)}_{\sim\theta_i}(\boldsymbol{\omega}) = \int_{\Gamma_{\sim\theta_i}} \left\{ y(\boldsymbol{\omega}, \boldsymbol{\theta}) - E^y_{\sim\theta_i}(\boldsymbol{\omega}) \right\}^n p_{\sim\theta_i} d\boldsymbol{\theta}_{\sim\theta_i}. \tag{14}$$

2.3. Moment-based global sensitivity analysis: Current system state

Considering the system under investigation at its current state in terms of the *operational* variables, i.e., $\boldsymbol{\theta} = \boldsymbol{\theta}^c$ (superscript c denoting the current deterministic configuration of the *operational* variables), we evaluate

$$\mathrm{AMA}E_{\omega_i}(\boldsymbol{\theta}^c) = \int_{\Gamma_{\omega_i}} \left| E^y_{\boldsymbol{\omega}}(\boldsymbol{\theta}^c) - E^y_{\sim\omega_i}(\boldsymbol{\theta}^c) \right| p_{\omega_i} d\omega_i, \tag{15}$$

$$\mathrm{AMA}SM^{(n)}_{\omega_i}(\boldsymbol{\theta}^c) = \int_{\Gamma_{\omega_i}} \left| SM^{y,(n)}_{\boldsymbol{\omega}}(\boldsymbol{\theta}^c) - SM^{y,(n)}_{\sim\omega_i}(\boldsymbol{\theta}^c) \right| p_{\omega_i} d\omega_i, \tag{16}$$

to quantify the sensitivity of the mean and the n-order statistical moments of y with respect to the *non-operational* variables ω_i. Note that indices (15)–(16) are the counterparts of (5)–(6) when we focus on the current state of the *operational* variables and we only retain the uncertainty in the *non-operational* variable.

2.4. Moment-based global sensitivity analysis: the operational picture

Considering a management/design perspective and following Dell'Oca (2023), we compute

$$\mathrm{AMA}E_{\theta_i}(\boldsymbol{\omega}) = \int_{\Gamma_{\theta_i}} |E^y_{\boldsymbol{\theta}}(\boldsymbol{\omega}) - E^y_{\sim\theta_i}(\boldsymbol{\omega})| p_{\theta_i} d\theta_i, \tag{17}$$

$$\mathrm{AMA}SM^{(n)}_{\theta_i}(\boldsymbol{\omega}) = \int_{\Gamma_{\theta_i}} |SM^{y,(n)}_{\boldsymbol{\theta}}(\boldsymbol{\omega}) - SM^{y,(n)}_{\sim\theta_i}(\boldsymbol{\omega})| p_{\theta_i} d\theta_i, \tag{18}$$

to quantify the sensitivity of the mean and the n-statistical moments of y with respect to the *operational* variable θ_i (while recognizing the lack of knowledge in the *non-operational* variables $\boldsymbol{\omega}$). Note that, AMA$E_{\theta_i}(\boldsymbol{\omega})$ and AMA$SM^{(n)}_{\theta_i}(\boldsymbol{\omega})$ are random global sensitivity indices due to their dependence on $\boldsymbol{\omega}$. Thus, it is possible to evaluate the whole pdf of *operational* sensitivity indices AMA$E_{\theta_i}(\boldsymbol{\omega})$ and AMA$SM^{(n)}_{\theta_i}(\boldsymbol{\omega})$. The pdf of an *operational* sensitivity index offers a comprehensive quantification of both the impact that θ_i has on a given statistical moment of y, and the associated uncertainty stemming from the lack of knowledge about $\boldsymbol{\omega}$. For example, a pdf of AMA$E_{\theta_i}(\boldsymbol{\omega})$ characterized by a distinct peak and a small variance indicates a low uncertainty (across the ensemble of realizations of $\boldsymbol{\omega}$) in the sensitivity of the mean of y to the *operational* variable θ_i. Conversely, a wide pdf of AMA$E_{\theta_i}(\boldsymbol{\omega})$ indicates a strong uncertainty in the impact of θ_i on the mean behavior of y.

As an example, Fig. 2 depicts the workflow for evaluating the pdf of AMA$E_{\theta_i}(\boldsymbol{\omega})$ when the model output y depends on three *non-operational* variables $\boldsymbol{\omega} = (\omega_1; \omega_2; \omega_3)$ and two *operational* variables $\boldsymbol{\theta} = (\theta_1; \theta_2)$. For a random realization of $\boldsymbol{\omega}$, we (*i*) sample $\boldsymbol{\theta}$ to compute $E^y_{\boldsymbol{\theta}}(\boldsymbol{\omega})$ (using Eq. (8)) and $E^y_{\sim\theta_i}(\boldsymbol{\omega})$ (using Eq. (13)) and (*ii*) evaluate the (random) sensitivity index AMA$E_{\theta_i}(\boldsymbol{\omega})$ (using Eq. (17)). Steps (*i*)-(*ii*) are repeated for an ensemble of realizations of $\boldsymbol{\omega}$ to evaluate the pdf of AMA$E_{\theta_i}(\boldsymbol{\omega})$. The same strategy is adopted to estimate the pdf of AMA$SM^{(n)}_{\theta_i}(\boldsymbol{\omega})$.

2.5. Probability of failure: Current system state and operational interventions

The exceedance probability introduced in Section 2.1 measures the likelihood that y exceeds the threshold k. Here, such an event is classified as a system failure and is hereafter denoted by the symbol $\times$, safe conditions being denoted by the symbol $\checkmark$. When assessing the current state of the system (i.e., for $\boldsymbol{\theta} = \boldsymbol{\theta}^c$), we define the probability of failure, $P^c_{\times}$, and non-failure (safety), $P^c_{\checkmark}$, of the system as

$$P^c_{\times} = Pr(y(\boldsymbol{\omega}, \boldsymbol{\theta}^c) \geq k), \qquad P^c_{\checkmark} = 1 - P^c_{\times}. \tag{19}$$

Fig. 3a depicts a sketch of diverse realizations of $\boldsymbol{\omega}$ (circles) distinguishing between those that correspond to system failure (red circles) from their counterparts associated with safe system states (green circles).

Following the methodology described in Section 2.1, we quantify the sensitivity of the probability of system failure with respect to the variability of ω_i when being at the current state through the following index

$$\mathrm{AMA}P^c_{\times,\omega_i} = \int_{\Gamma_{\omega_i}} \left| P^c_{\times} - P^c_{\times,\sim\omega_i} \right| p_{\omega_i} d\omega_i, \tag{20}$$

where $P^c_{\times,\sim\omega_i}$ is the probability of failure at the current system state conditional to ω_i.

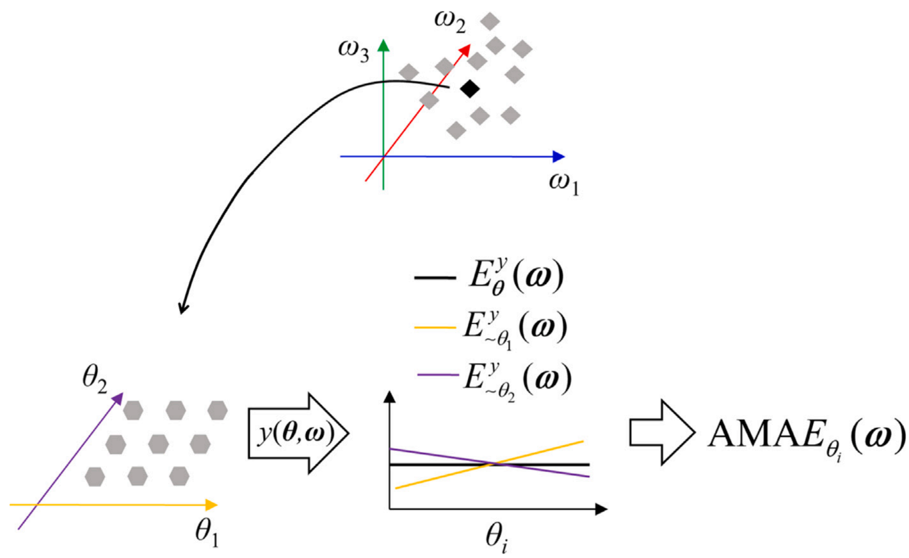

Fig. 2. Workflow for the evaluation of the pdf of $\mathrm{AMA}E_{\theta_i}(\boldsymbol{\omega})$. (For interpretation of the references to color in this figure legend, the reader is referred to the web version of this article.)

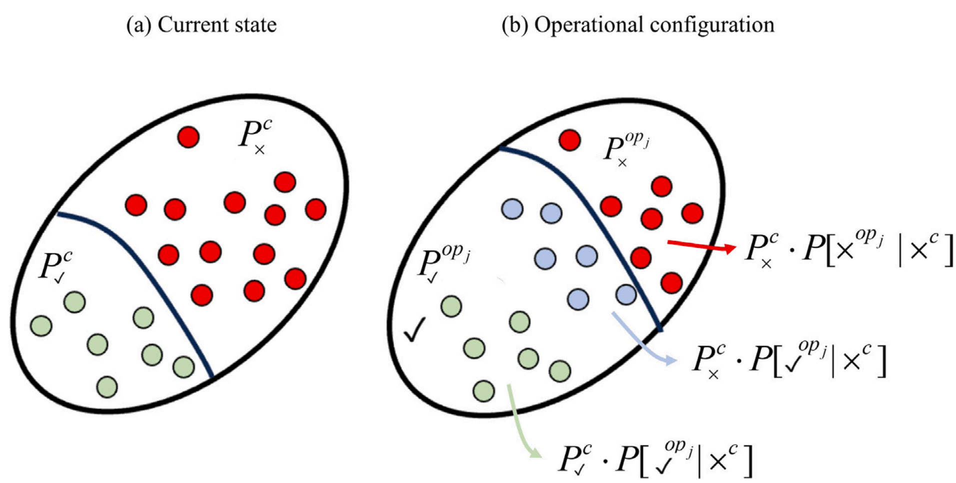

Fig. 3. Sketch of the ensemble of random realizations of $\boldsymbol{\omega}$ at (a) the current state and (b) under an *operational* intervention. Considering the current state, the system can either fail (red circle) or remain functional (green circle). After the operational intervention, there are realizations where the system transitions from failing to safe conditions (blue circles). (For interpretation of the references to color in this figure legend, the reader is referred to the web version of this article.)

Considering jointly the uncertainty in both $\boldsymbol{\omega}$ and possible operational interventions (i.e., design variability in $\boldsymbol{\theta}$), the (unconditional) probabilities of failure, $P_{\times}^{op}$, and safety, $P_{\checkmark}^{op}$, are defined as

$$P_{\times}^{op} = Pr(y(\boldsymbol{\omega},\boldsymbol{\theta}) \geq k), \qquad P_{\checkmark}^{op} = 1 - P_{\times}^{op}. \tag{21}$$

It is also possible to define the probabilities of failure, $P_{\times}^{op}(\boldsymbol{\omega})$, and safety, $P_{\checkmark}^{op}(\boldsymbol{\omega})$, for a generic realization of the *non-operational* variable $\boldsymbol{\omega}$ as

$$P_{\times}^{op}(\boldsymbol{\omega}) = Pr(y(\sim\boldsymbol{\omega},\boldsymbol{\theta}) \geq k), \qquad P_{\checkmark}^{op}(\boldsymbol{\omega}) = 1 - P_{\times}^{op}(\boldsymbol{\omega}), \tag{22}$$

where both $P_{\times}^{op}(\boldsymbol{\omega})$ and $P_{\checkmark}^{op}(\boldsymbol{\omega})$ are random quantities, due to the randomness in $\boldsymbol{\omega}$. Following the methodological steps outlined in Section 2.4, here we introduce the probability-based global sensitivity indices within the operational picture as

$$\mathrm{AMA}P_{\theta_i}(\boldsymbol{\omega}) = \int_{\Gamma_{\theta_i}} \left| P_{\times}^{op}(\boldsymbol{\omega}) - P_{\times,\sim\theta_i}^{op}(\boldsymbol{\omega}) \right| p_{\theta_i} d\theta_i, \tag{23}$$

where $P_{\times,\sim\theta_i}^{op}(\boldsymbol{\omega})$ is the probability of failure conditional to ith *operational* variable θ_i in the generic random realization $\boldsymbol{\omega}$. It is important to note that, $\mathrm{AMA}P_{\theta_i}(\boldsymbol{\omega})$ is a random global sensitivity index due to its dependence on $\boldsymbol{\omega}$ and quantifies the sensitivity of the probability of failure with respect to the *operational* variable θ_i within a single realization of $\boldsymbol{\omega}$. Thus, it is possible to assess the pdf of $\mathrm{AMA}P_{\theta_i}(\boldsymbol{\omega})$ to inspect the sensitivity of the probability of failure to the *operational* variable θ_i, across the whole ensemble of realizations of $\boldsymbol{\omega}$. Note that the evaluation workflow for $\mathrm{AMA}P_{\theta_i}(\boldsymbol{\omega})$ is patterned after that for $\mathrm{AMA}E_{\theta_i}(\boldsymbol{\omega})$ illustrated in Fig. 2.

When considering a potential intervention (i.e., the choice of a specific configuration $\boldsymbol{\theta} = \boldsymbol{\theta}^j$ of the *operational* variables) in an existing system, it is important to quantify the benefit of this choice as compared to the current system state $\boldsymbol{\theta}^c$. This evaluation can be carried out using the law of total probability according to which the probability of system failure after intervention, $P_{\times}^{op_j} = Pr(y(\boldsymbol{\omega},\boldsymbol{\theta}^j) \geq k)$, can be computed as

$$P_{\times}^{op_j} = P_{\times}^{c} \cdot P_{[\times^{op_j}|\times^c]} + P_{\checkmark}^{c} \cdot P_{[\times^{op_j}|\checkmark^c]}, \tag{24}$$

where $P_{[\times^{op_j}|\times^c]}$ is the probability of failure after intervention if the system is failing in its current state. Such quantity quantifies the probability that setting $\boldsymbol{\theta}^j$ will not prevent y from exceeding the threshold k when failure is occurring in the current system state. The term $P_{[\times^{op_i}|\checkmark^c]}$ is the probability that the system fails after intervention even though the system is not failing in its current state. It represents the probability

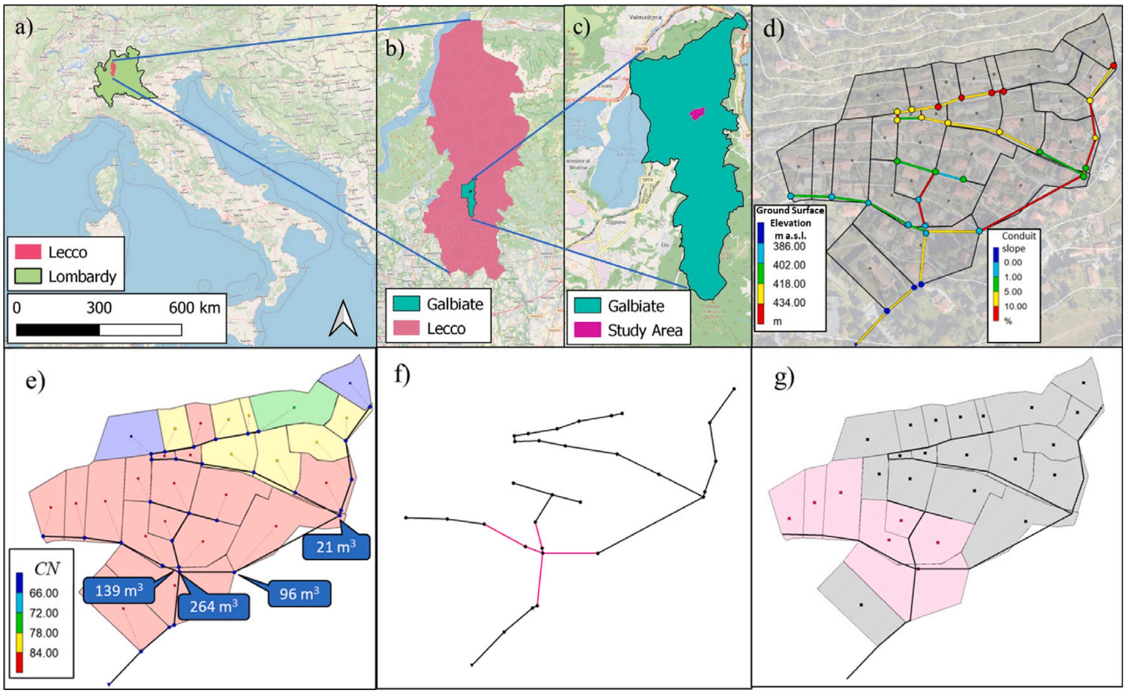

Fig. 4. Study area, location within (a) Italy and the Lombardy Region, (b) Lecco Province and (c) the municipality of Galbiate. (d) Network conduits, their slopes and elevation of the ground surface. (e) Network nodes with the indication of flood volumes following a 1-h rainfall event with a 10-years return period. (f) Conduit network, highlighting (in pink) conduits whose diameter and roughness are considered as *operational* quantities in our study. (g) Sub-catchments forming the study area, highlighting (in pink) those in which infiltration attributes (i.e., CN values) are considered as *operational* quantities in our study. (For interpretation of the references to color in this figure legend, the reader is referred to the web version of this article.)

that the intervention yields negative impacts, causing the system to fail despite being safe in its current state.

In a similar way, one can evaluate the probability of safety after the intervention, $P_{\checkmark}^{op_j} = 1 - P_{\times}^{op_j}$, as

$$P_{\checkmark}^{op_j} = P_{\times}^{c} \cdot P_{[\checkmark^{op_j}|\times^c]} + P_{\checkmark}^{c} \cdot P_{[\checkmark^{op_j}|\checkmark^c]}, \tag{25}$$

where $P_{[\checkmark^{op_j}|\times^c]}$ is the probability of achieving safety after the intervention when the system is failing in its current state. This quantity measures the likelihood that setting θ^j will shift the system from failure to safe conditions. Note that this term can be employed to represent the effectiveness of the intervention. The term $P_{[\checkmark^{op_j}|\checkmark^c]}$ in Eq. (25) is the probability of maintaining safety after the intervention when the system is already safe in its current state. Formulations (24) and (25) are elucidated in Fig. 3b for $P_{[\times^{op_j}|\checkmark^c]} = 0$ (i.e, in the typical case of non-harmful interventions).

Finally, to grasp the intensity of the *non-operational* variables for which the system fails or it is safe at the current state θ^c and after the intervention θ^j, we introduce the expected value of the ith *non-operational* variable ω_i conditional to system failure and safety, respectively defined as

$$E_{\times}^{\omega_i,\alpha} = \int_{\Gamma_{\omega_i}} \omega_i p_{\omega_i,\times^\alpha} d\omega_i; \qquad E_{\checkmark}^{\omega_i,\alpha} = \int_{\Gamma_{\omega_i}} \omega_i p_{\omega_i,\checkmark^\alpha} d\omega_i, \tag{26}$$

with $\alpha = c, op_j$. Here $p_{\omega_i,\times^\alpha}$ is the pdf of ω_i when the system fails at the current state (for $\alpha = c$) and after the intervention (for $\alpha = op_j$). Whereas $p_{\omega_i,\checkmark^\alpha}$ is its counterpart when the system does not fail.

2.6. Modeling approach

We rest on a description of the rainfall event grounded on the widely used power-law formulation (Burlando & Rosso, 1996)

$$h_{d,T_R} = h_{1,T_R} d^n, \tag{27}$$

where h_{d,T_R} $[L]$ is the rainfall depth related to an event with return period T_R $[T]$ and duration d $[T]$, h_{1,T_R} $[LT^{-n}]$ is its counterpart associated with unit rain duration, and n $[-]$ is a scaling coefficient. Rainfall intensity is simulated according to the Chicago hyetograph with a centered peak.

The Storm Water Management Model — SWMM (Arjenaki, Sanayei, Heidarzadeh, & Mahabadi, 2021; Mohammed, Zwain, & Hassan, 2021; Rossman, 2010) is employed to evaluate surface runoff, water infiltration and flow within the sewer system associated with the area we consider as a testbed for our approach (see Section 2.7). The urban catchment is conceptualized as the collection of sub-catchments, each characterized by its surface area A_i $[L^2]$, representative width W_i $[L]$, storage capacity (per unit area) δ_{si} $[L]$, and slope S_i $[-]$.

Infiltration is evaluated via the widely used Curve Number method (Boughton, 1989). The latter quantifies the volume of rainfall infiltrating into the soil (per unit value of A_i during the time step Δt), $F_i[L]$, as

$$F_i = h_{\Delta t} - \frac{(h_{\Delta t})^2}{h_{\Delta t} + S_{max}}, \text{ with } S_{max} = \frac{C_1}{CN_i} - C_2, \tag{28}$$

where $h_{\Delta t}$ $[L]$ is the rainfall depth during time step Δt, S_{max} $[L]$ is the soil maximum moisture storage capacity, C_1 and C_2 are constants (in the metric system units: $C_1 = 25400$ mm and $C_2 = 250$ mm), and CN_i is a dimensionless parameter ranging from 0 to 100. Sub-catchments characterized by high values of CN are associated with reduced infiltration capacity and vice versa. It is worth noting that our focus is on high-intensity precipitation events occurring across temporal windows of minutes or hours. Thus, the contributions of evaporation are neglected.

The runoff of the ith sub-catchment Q_i is evaluated according to the Manning formulation, i.e.

$$Q_i = \frac{S_i^{1/2} R_i^{5/3} W_i}{n_{s,i}}, \tag{29}$$

where $n_{s,i}$ $[T/L^{1/3}]$ is the roughness coefficient associated with the ith sub-catchment, $R_i = \delta_i - \delta_{si}$ $[L]$, and δ_i and W_i are, respectively, the height of the water and the width of the equivalent (in terms of Q_i) rectangular channel representing the ith sub-catchment.

The sewer network is conceptualized as a set of nodes and conduits that receive the runoff from pertinent sub-catchments. Flow in each conduit of the sewer network is solved according to Dynamic Wave formulations specifically tailored for closed conduits (Rossman, 2017). As system variables, key geometric attributes of the sewer network are required: land surface elevation z_j $[L]$ and depth ζ_j $[L]$ of the jth node of the sewer network, as well as length L_k $[L]$, diameter ϕ_k $[L]$, and roughness $n_{c,k}$ $[T/L^{1/3}]$ of the kth conduit. A flooding event occurs at node j when the hydraulic head therein exceeds ζ_j. Temporal integration of the spill flow rates associated with a rain event determines the flood volume FV_j $[L^3]$ at the jth node. The sum of FV_j at all flooded nodes in an area of interest yields the overall flood volume, FV $[L^3]$. The latter represents our model output of interest (i.e., $y = FV$), for which we assess the sensitivity to the *operational* and *non-operational* variables.

2.7. Study area

We illustrate our approach on an urban catchment located in the municipality of Galbiate (Northen Italy, Lombardy Region, Lecco Province, see Fig. 4(a–c)). Galbiate is nested in a mountainous region, with elevations between 225 and 922 m above sea level. It has a population of about 8400 people with a population density of 540 people per square kilometer. The study area spans 8.30 hectares and is served by a sewer network consisting of 30 conduits (total length 1.34 km), 30 collection nodes and 1 outlet node (see Fig. 4d). The catchment is characterized by rather high values of CN (see Fig. 4e) reflecting a rather low infiltration capacity of the area. This characteristic prompted sewer system managers to identify it as an area of interest, after preliminary investigations revealed possible flooding in the area during heavy rainfall events. As an example, Fig. 4e depicts the flood volumes FV_j at the most critical sewer nodes, evaluated for a rainfall event characterized by $T_R = 10$ years and $d = 1$ hour.

Here, we focus on the area highlighted in 4g, where flooding events are more severe under the current state of the system. We then tie our work to the preliminary design phase of future interventions to quantify the impact of *operational* variables (elements on which actions can be taken) on the magnitude of the flood, while accounting for the uncertain nature of the urban catchment features. In line with standard sewer systems intervention practices, we focus on the following operational variables:

- Roughness, n_c, and diameter, ϕ, of the six conduits embedded in the flooded area (see Fig. 4f). Increasing ϕ as well as decreasing n_c result in a reduction (at a fixed flow rate) in the hydraulic head within the sewer conduits, thus mitigating the risk of flooding.
- CN coefficient of the seven sub-catchments forming the flooded area (see Fig. 4g). Decreasing CN, by for example modifying the coverage of the sub-catchments, enhances their infiltration capacity, thus reducing the incoming flow to the sewer system. Here, the idea of intervening on CN stems from the observation that, at the current state, these sub-catchments are characterized by low infiltration capacity (see Fig. 4e).

To account for incomplete knowledge of the features of the urban catchment and of the rainfall event, we consider the following *non-operational* variables, whose estimates are prone to high uncertainty (de Michele, Rosso, & Rulli, 2005; Yu & Coulthard, 2015):

- Rainfall depth, h_{1,T_R} (for the unit rain duration) and duration, d. The estimation of h_{1,T_R} variability (or support) is based on an uncertainty propagation analysis performed on the equations describing the rainfall probability indicator lines specific to the region of interest (de Michele et al., 2005). The rainfall duration is chosen to fall within the range of 15–60 min, in line with the common occurrence of intense precipitation events in the area.

Table 1
Ranges of variability for uncertain variables and values for deterministic model inputs employed in the study.

Variable - Symbol	Units	Type	Value
Conduit roughness[a] - n_c	s/m$^{1/3}$	*Operational*	0.009, 0.014
Conduit diameter[a] - ϕ	m	*Operational*	0.3, 0.4, 0.5, 0.6
CN reduction[b] - CN_r	–	*Operational*	5, 10, 15
Rainfall depth - $h_{1,10}$	mm	*Non-operational*	[30–55]
Rainfall duration - d	min	*Non-operational*	[15–60]
Surface roughness - n_s	s/m$^{1/3}$	*Non-operational*	[0.01–0.25]
Storage capacity - δ_s	mm	*Non-operational*	[0–10]
Return period - T_R	years	Fixed	10
Peak position - r	–	Fixed	0.5
Surface slope - S_i	–	Fixed	Sup. Material
Surface area - A_i	m^2	Fixed	Sup. Material
Surface width - W_i	m	Fixed	Sup. Material
Surface elevation - z_j	m	Fixed	Sup. Material
Node depth - ζ_j	m	Fixed	Sup. Material
Conduit length - L_k	m	Fixed	Sup. Material

[a] Only for the conduits highlighted in pink in Fig. 4f.
[b] Only for the sub-catchments highlighted in pink in Fig. 4g.

- Roughness coefficient, n_s and the storage capacity, δ_s, of the sub-catchments. The support of n_s is selected on the basis of typical roughness coefficients for urban catchments (Rossman, 2010). The storage capacity support is assessed according to the slope of the sub-catchments (Kidd, 1978; Rossman, 2010; Viessman & Lewis, 2003).

Table 1 lists (i) plausible values of the *operational* variables, $\boldsymbol{\theta} = (n_c, \phi, CN$ reduction), each treated here as a discrete random quantity, and (ii) support ranges (selected as described above) of the *non-operational* variables, $\boldsymbol{\omega} = (h_{1,10}, d, n_s, \delta_s)$, here treated as continuous random variables. Both $\boldsymbol{\theta}$ and $\boldsymbol{\omega}$ are assumed to have a uniform pdf across their supports. This allows us to assign equal weight to all values of $\boldsymbol{\theta}$ or $\boldsymbol{\omega}$ within their respective supports. For illustration purposes, we assume that each *non-operational* variable is homogeneous in space. If data are available regarding the shape of the pdf of $\boldsymbol{\theta}$ and/or $\boldsymbol{\omega}$ as well as the spatial variability of $\boldsymbol{\theta}$, this information can be readily included in our workflow. Moreover, since $d < 60$ min (as is typical for extreme events), we set $n = 1$ in Eq. (27). For completeness, Table 1 also lists system variables that we consider as deterministically known and/or that are not considered in the context of future interventions. Note that we set $T_R = 10$ years, as usually required by local regulating bodies.

3. Results and discussion

In the following (Sections 3.1 and 3.3), we start by illustrating, making use of the deterministic moment-based (15) and the probability-based (20) sensitivity indices, the impact of the *non-operational* variables $\boldsymbol{\omega} = (h_{1,10}, d, n_s, \delta_s)$ on the total flood volume, FV, for the setting illustrated in Section 2.7 at the current state of the system, $\boldsymbol{\theta} = \boldsymbol{\theta}^c$. This task is performed by relying on a Monte Carlo (MC) strategy to sample the stochastic four-dimensional $\Gamma_{\boldsymbol{\omega}}$ space.

Sections 3.2 and 3.4 are devoted to our investigation of the sensitivity of FV to the *operational* variables $\boldsymbol{\theta} = (n_c, \phi, CN_r)$, while considering uncertainty in $\boldsymbol{\omega}$. The study involves the use of both (random) moment-based (17)–(18) and (random) probability-based (23) sensitivity indices, collectively aiming to capture diverse complementary aspects of the variability in FV. We recall that, the *operational* sensitivity analysis requires these steps: (i) draw a realization $\boldsymbol{\omega}$ of the *non-operational* variables; (ii) evaluate the (random) sensitivity indices (17)–(18) and (23) at all possible combinations of the *operational* variables; (iii) repeat steps (i)-(ii) for all the realizations of $\boldsymbol{\omega}$ (we employ the same MC realizations employed to sample $\Gamma_{\boldsymbol{\omega}}$ introduced above) and evaluate the pdf of all random sensitivity indices. Stable results are achieved by relying on 5×10^4 realizations of $\boldsymbol{\omega}$ for set (i.e., 24) of the *operational* variables. Thus, a total of 1.2×10^6 model evaluations

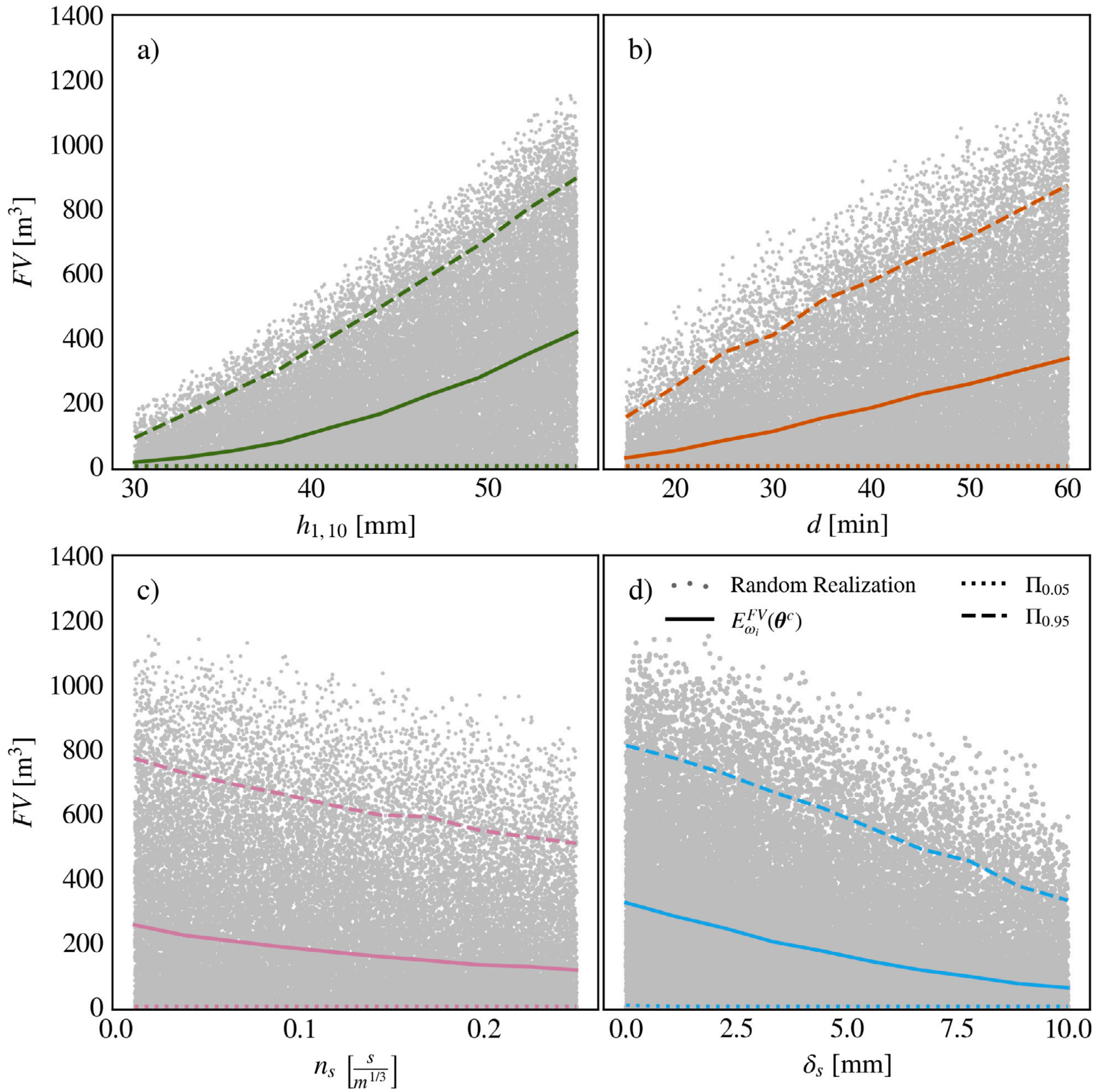

Fig. 5. Ensemble of random realizations of $FV(\boldsymbol{\omega}, \theta^c)$ (gray dots) versus $\omega_i = ((a)h_{1,10}; (b)d; (c)n_s; (d)\delta_s)$. The conditional mean of the flooding volume at the current system state, $E^{FV}_{\omega_i}(\theta^c)$ (solid curve) as well as the 5th, $\Pi_{0.05}$, and 95th, $\Pi_{0.95}$, percentiles (dotted curves) are also included.

have been performed in our study. All computations are performed upon relying on an Intel Core i9-13900KF processor and 128Gb RAM, the average time per simulation being approximately 0.05 s. Note that in instances involving prediction models which computational burden may be unaffordable, surrogate modeling techniques can be used within our approach (e.g., Dell'Oca, Guadagnini and Riva, 2020; Dell'Oca et al., 2017; Zeighami, Sandoval, Guadagnini, & Di Federico, 2023).

3.1. Current system state: Moment-based GSA

In this section, we focus on the GSA of FV with respect to the *non-operational* variables $\boldsymbol{\omega} = (h_{1,10}, d, n_s, \delta_s)$, given the current system θ^c. Assessing the sensitivity of the statistical moments of FV to each *non-operational* variable ω_i allows to establish the most relevant sources of uncertainty (embedded in $\boldsymbol{\omega}$) in predicting flood volume at the current system state. The objective of this analysis is to address the following questions 'Given the current state of the system, how significant is the impact of the inherent uncertainty in rainfall event attributes and urban catchment drainage characteristics on the statistical moments of the total flood volume?' and 'What investigations aimed at reducing uncertainty should be prioritized to improve reliability of flood volume predictions?'.

Fig. 5 depicts the entire collection of random realizations of flood volume, $FV(\boldsymbol{\omega}, \theta^c)$, highlighting their dependence on each component of $\boldsymbol{\omega}$ (i.e., $\omega_i = (a)h_{1,10}$; $(b)d$; $(c)n_s$; and $(d)\delta_s$). The expected value of FV conditional to each ω_i, $E^{FV}_{\sim\omega_i}(\theta^c)$, is also included in each plot (solid curve) as well as the confidence bounds associated with the 0.05 and 0.95 percentiles. Despite the significant variability exhibited by FV, which stems from the uncertainty associated with $\boldsymbol{\omega}$, the overall trend displayed by the results is consistent with typical expectations. Heavy rainfall events and/or long rain durations lead to increased FV (see Fig. 5a, b). Conversely, urban basins that are rougher (i.e., associated with high n_s values) and/or are characterized by higher storage capacity (i.e, high δ_s) yield reduced FV values (see Fig. 5c,d).

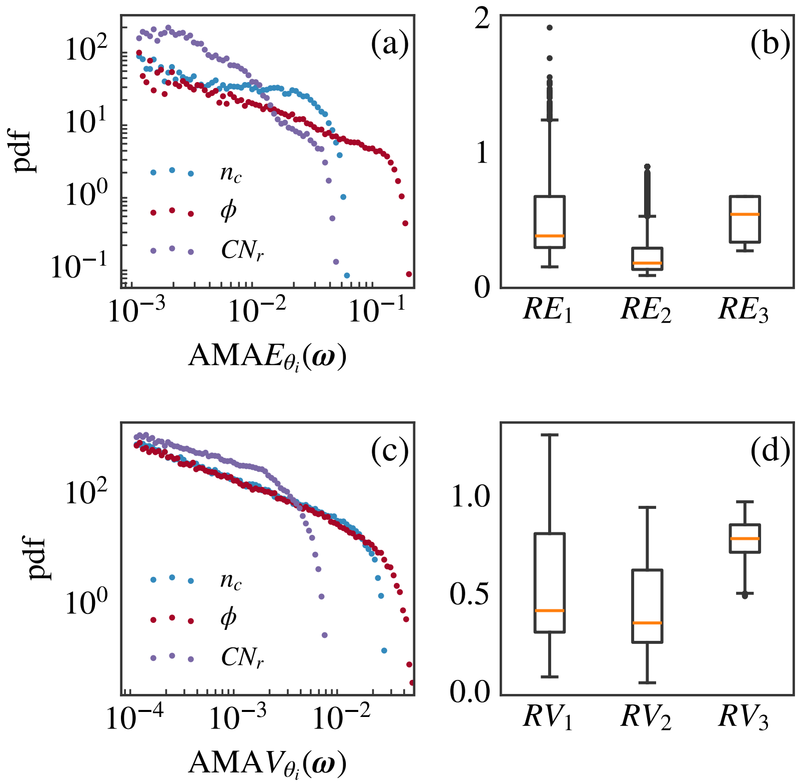

Fig. 6. Probability density function of (a) $\mathrm{AMA}E_{\theta_i}(\boldsymbol{\omega})$ and (c) $\mathrm{AMA}V_{\theta_i}(\boldsymbol{\omega})$, for $\theta_i = (n_c, \phi, CN_r)$. Ratios (b) $RE_1 = \mathrm{AMA}E_{CN_r}(\boldsymbol{\omega})/\mathrm{AMA}E_{n_c}(\boldsymbol{\omega})$, $RE_2 = \mathrm{AMA}E_{CN_r}(\boldsymbol{\omega})/\mathrm{AMA}E_{\phi}(\boldsymbol{\omega})$, and $RE_3 = \mathrm{AMA}E_{n_c}(\boldsymbol{\omega})/\mathrm{AMA}E_{\phi}(\boldsymbol{\omega})$, and (d) $RV_1 = \mathrm{AMA}V_{CN_r}(\boldsymbol{\omega})/\mathrm{AMA}V_{n_c}(\boldsymbol{\omega})$, $RV_2 = \mathrm{AMA}V_{CN_r}(\boldsymbol{\omega})/\mathrm{AMA}V_{\phi}(\boldsymbol{\omega})$, and $RV_3 = \mathrm{AMA}V_{n_c}(\boldsymbol{\omega})/\mathrm{AMA}V_{\phi}(\boldsymbol{\omega})$. (For interpretation of the references to color in this figure legend, the reader is referred to the web version of this article.)

Table 2
Global sensitivity indices $\mathrm{AMA}E_{\omega_i}(\theta^c)$ and $\mathrm{AMA}V_{\omega_i}(\theta^c)$ associated with the *non-operational* variable ω_i, given the current state of system θ^c.

ω_i	$\mathrm{AMA}E_{\omega_i}(\theta^c)$	$\mathrm{AMA}V_{\omega_i}(\theta^c)$
$h_{1,10}$	0.68	0.57
d	0.50	0.51
n_s	0.22	0.22
δ_s	0.43	0.35

Table 3
Operational moment-based global sensitivity indices: mean and standard deviation, $\mathrm{AMA}E^{op}_{\theta_i} \pm \sigma^{op}_{\mathrm{AMA}E_{\theta_i}}$, of $\mathrm{AMA}E_{\theta_i}(\boldsymbol{\omega})$, and mean and standard deviation, $\mathrm{AMA}V^{op}_{\theta_i} \pm \sigma^{op}_{\mathrm{AMA}V_{\theta_i}}$, of $\mathrm{AMA}V_{\theta_i}(\boldsymbol{\omega})$ for $\theta_i = (n_c, \phi, CN_r)$.

θ_i	$\mathrm{AMA}E^{op}_{\theta_i} \pm \sigma^{op}_{\mathrm{AMA}E_{\theta_i}}$ [$\times 10^{-3}$]	$\mathrm{AMA}V^{op}_{\theta_i} \pm \sigma^{op}_{\mathrm{AMA}V_{\theta_i}}$ [$\times 10^{-3}$]
n_c	9.9 ± 12.8	2.5 ± 4.5
ϕ	26.9 ± 40.0	3.4 ± 6.7
CN_r	4.3 ± 7.1	0.7 ± 1.1

Table 2 lists the moment-based GSA metrics suitable for quantifying the sensitivity of mean, $\mathrm{AMA}E_{\omega_i}(\theta^c)$ (Eq. (15)), and variance $\mathrm{AMA}V_{\omega_i}(\theta^c)$ (Eq. (16) with $n = 2$) of FV with respect to each of the *non-operational* variables. Although Table 2 reveals that all *non-operational* variables considered impact the prediction of the mean flood volume and the associated uncertainty (measured by its variance), its analysis allows for planning future experimental activities. Priority should be given to improving our understanding of the features of rainfall events (i.e., on the characterization of $h_{1,10}$ and d). Subsequently, attention could be directed toward the characterization of the storage capacity of the catchment, followed by its surface roughness.

3.2. Operational interventions: Moment-based operational GSA

Here, we focus on the moment-based GSA of FV with respect to the *operational* variables $\boldsymbol{\theta} = (n_c, \phi, CN_r)$. The main goal is to assess the strength with which each *operational* variable θ_i impacts the flood volume when the urban catchment and rain attributes, $\boldsymbol{\omega}$, are uncertain.

Fig. 6 depicts the pdf of (*a*) $\mathrm{AMA}E_{\theta_i}(\boldsymbol{\omega})$ (Eq. (17)) and (*c*) $\mathrm{AMA}V_{\theta_i}(\boldsymbol{\omega})$ (Eq. (18) with $n = 2$), for $\theta_i = n_c, \phi, CN_r$. Results are complemented by the boxplots of the ratios (b) $RE_1 = \mathrm{AMA}E_{CN_r}(\boldsymbol{\omega})/\mathrm{AMA}E_{n_c}(\boldsymbol{\omega})$, $RE_2 = \mathrm{AMA}E_{CN_r}(\boldsymbol{\omega})/\mathrm{AMA}E_{\phi}(\boldsymbol{\omega})$, and $RE_3 = \mathrm{AMA}E_{n_c}(\boldsymbol{\omega})/\mathrm{AMA}E_{\phi}(\boldsymbol{\omega})$, as well as (d) $RV_1 = \mathrm{AMA}V_{CN_r}(\boldsymbol{\omega})/\mathrm{AMA}V_{n_c}(\boldsymbol{\omega})$, $RV_2 = \mathrm{AMA}V_{CN_r}(\boldsymbol{\omega})/\mathrm{AMA}V_{\phi}(\boldsymbol{\omega})$, and $RV_3 = \mathrm{AMA}V_{n_c}(\boldsymbol{\omega})/\mathrm{AMA}V_{\phi}(\boldsymbol{\omega})$. Fig. 6 is complemented by Table 3 which displays mean, $\mathrm{AMA}E^{op}_{\theta_i}$, and standard deviation, $\sigma^{op}_{\mathrm{AMA}E_{\theta_i}}$, of $\mathrm{AMA}E_{\theta_i}(\boldsymbol{\omega})$, as well as mean, $\mathrm{AMA}V^{op}_{\theta_i}$, and standard deviation, $\sigma^{op}_{\mathrm{AMA}V_{\theta_i}}$, of $\mathrm{AMA}V_{\theta_i}(\boldsymbol{\omega})$. Note that $\mathrm{AMA}E^{op}_{\theta_i}$ quantifies the average (across the realizations of $\boldsymbol{\omega}$) impact of θ_i on predicting the mean flood volume, while $\sigma^{op}_{\mathrm{AMA}E_{\theta_i}}$ provides a measure of how this mean prediction is affected by uncertainty due to our lack of knowledge in $\boldsymbol{\omega}$. Similarly, $\mathrm{AMA}V^{op}_{\theta_i}$ quantifies the average impact of θ_i on flood volume variability (represented by its variance) and $\sigma^{op}_{\mathrm{AMA}V_{\theta_i}}$ is an indicator of how this variability is affected by uncertainty in $\boldsymbol{\omega}$.

Variations in the diameter ϕ of the conduits of the sewer system (see Fig. 6a and Table 3) yield the most relevant changes in the expected value of FV, as clearly visible by the pronounced right tail in the pdf of $\mathrm{AMA}E_{\phi}(\boldsymbol{\omega})$, and the relatively large value of $\mathrm{AMA}E^{op}_{\phi}$. However, this impact is associated with high variability across the ensemble of realizations $\boldsymbol{\omega}$, as quantified by $\sigma_{\mathrm{AMA}E_{\phi}}$. Conversely, the *operational* variables n_c and CN_r yield a reduced degree of uncertainty (i.e., more compact supports of the pdf of $\mathrm{AMA}E_{n_c}(\boldsymbol{\omega})$ and $\mathrm{AMA}E_{CN_r}(\boldsymbol{\omega})$) and exert a smaller influence on the expected value of FV. This result is further elucidated in Fig. 6b. Since RE_2 and RE_3 are always smaller

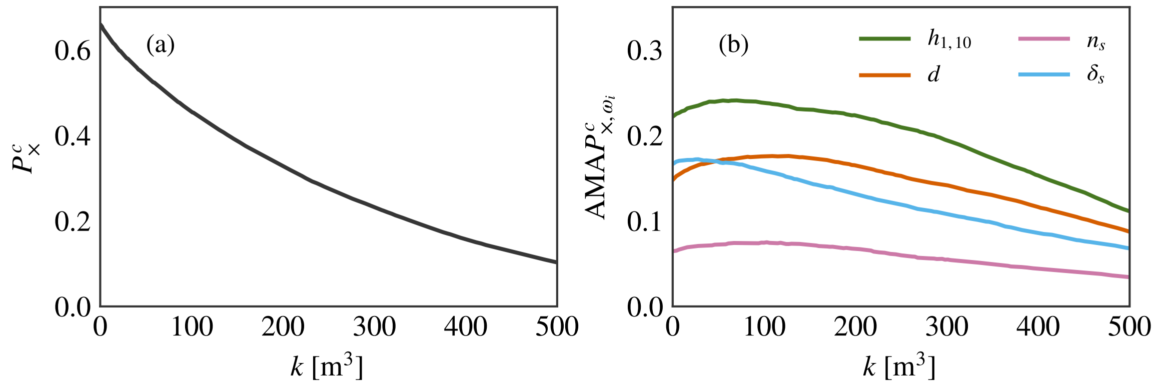

Fig. 7. (a) Probability of system failure $P^c_\times$ at the current system state, θ^c, versus the threshold flooding volume, k. (b) Probability-based sensitivity index of the probability of failure at the current system state, AMA$P^c_{\times,\omega_i}$ for $\omega_i = (h_{1,10}, d, n_s, \delta_s)$, versus k. (For interpretation of the references to color in this figure legend, the reader is referred to the web version of this article.)

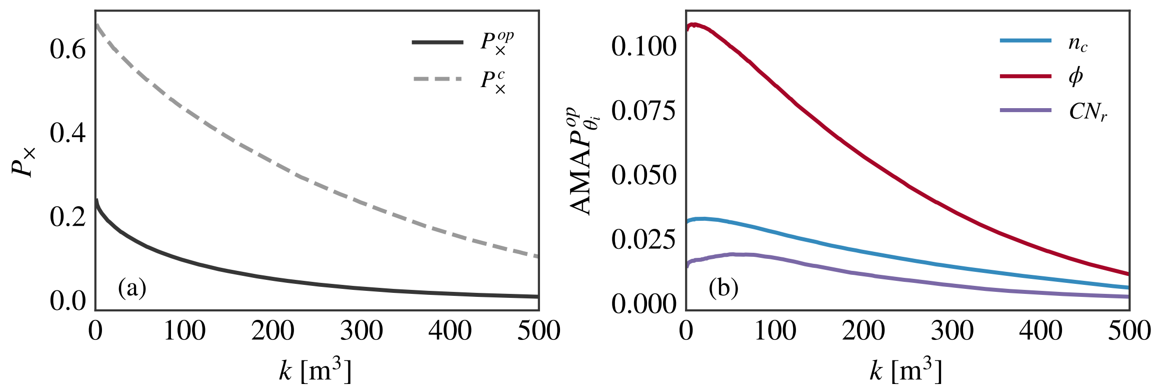

Fig. 8. (a) Unconditional probability of system failure, $P^{op}_\times$ (solid curve), considering all possible values of the *operational* variables and the uncertainty in the *non-operational* variables, versus the threshold k and the counterpart, $P^c_\times$ (dashed gray curve), evaluated at the current system state. (b) Operational probability-based sensitivity index, AMA$P^{op}_{\theta_i}$, versus the threshold k for $\theta_i = (n_c, \phi, CN_r)$. (For interpretation of the references to color in this figure legend, the reader is referred to the web version of this article.)

than one, variations in ϕ always have a larger impact on the expected value of FV as compared to variations in n_c and/or CN_r. Additionally, values of RE_1 reveal that the expected value of FV is overall more sensitive to variations in n_c than to those in CN_r, the opposite behavior (i.e., $RE_1 > 1$) being observed only for a few realizations of $\boldsymbol{\omega}$.

Considering the variance of FV (see Fig. 6c and Table 3), the least important parameter is CN_r, while ϕ and n_c have a similar impact. Note that the pdf of AMA$V_{CN_r}(\boldsymbol{\omega})$ is characterized by a smaller support than the pdfs associated with ϕ and n_c. This finding suggests that there is less uncertainty (across the realizations of $\boldsymbol{\omega}$) about the influence of CN_r on the variability of FV than what can be observed with reference to ϕ and n_c. Moreover, Fig. 6d reveals that variations in ϕ (see RV_2 and RV_3) are always the most important (in a relative sense) in defining the variance of FV across the ensemble of $\boldsymbol{\omega}$, while variations of CN_r are the least influential as quantified by RV_1.

In summary, our results reveal that the diameter of the sewer conduits is the dominant *operational* variable affecting both the expected value and the variability (as rendered through the variance) of the flood volume, given the range of possible realizations of the *non-operational* variables. This finding suggests that optimizing the value of ϕ should be the starting point of any intervention aimed at improving the system performance in the target area. Moreover, the effect of ϕ on both the mean and variance of FV is associated with a high degree of uncertainty across the ensemble of realizations of $\boldsymbol{\omega}$. This implies that efforts aimed at reducing the uncertainty inherent in $\boldsymbol{\omega}$ can yield substantial improvement in our understanding of how ϕ influences the system. Such insights are critically important for developing interventions aimed at enhancing system performance under uncertainty.

3.3. Current system state: Probability-based GSA

This Section is keyed to the analysis of the probability of system failure $P^c_\times$, Eq. (19), given the current configuration of the *operational* variables. Fig. 7a depicts $P^c_\times$ as a function of the threshold flooding volume k, which represents the maximum flood water allowable under safe conditions. Fig. 7b depicts the sensitivity index of the probability of failure, AMA$P^c_{\times,\omega_i}$ (Eq. (20)), for $\omega_i = (h_{1,10}, d, n_s, \delta_s)$, versus k. The probability of failure is markedly influenced by $h_{1,10}$, followed by (in decreasing order of importance) d, δ_s, and n_s. An exception is noted for $k < 44$ m^3 for which δ_s is slightly more influential than d on $P^c_\times$. These results are in line with findings reported in Section 3.1. Moreover, one can observe that AMA$P^c_{\times,\omega_i}$ consistently decreases with k when $k > 200$ m^3, suggesting that the probability of large flooding events exhibit reduced sensitivity to the uncertainty in *non-operational* variables.

3.4. Operational interventions: Probability-based operational GSA

The main objective of this Section is to assess the strength with which each *operational* variable θ_i impacts the probability of system failure, when $\boldsymbol{\omega}$ is uncertain. This analysis aims to address questions such as "Considering the uncertainty about the rainfall event attributes and urban catchment characteristics, which *operational* variable has the greatest impact on the probability of system failure?" and "How effective are diverse combinations of the *operational* variables in mitigating the probability of system failure?".

Fig. 8a juxtaposes the unconditional probability of system failure, $P^{op}_\times$ (Eq. (21)), and the probability of system failure at the current system state, $P^c_\times$ (Eq. (19)), versus the threshold flooding volume k. All

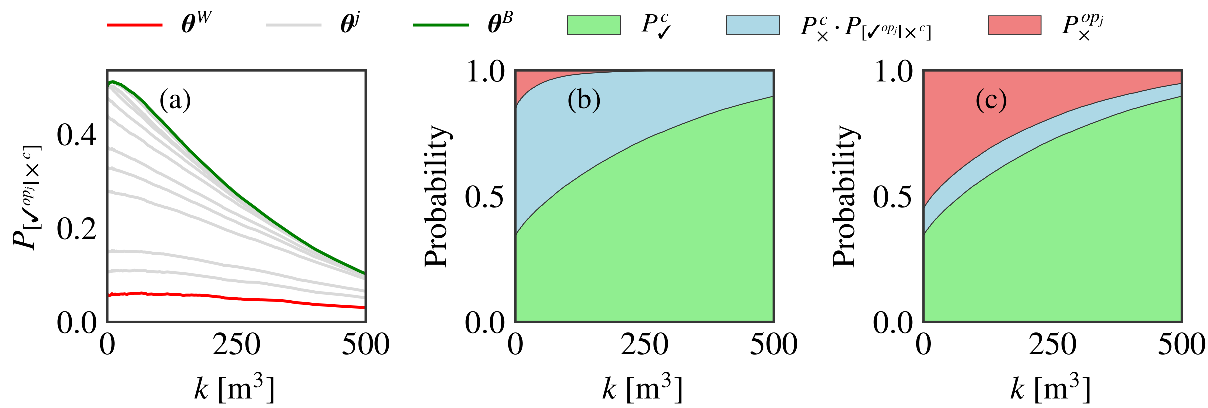

Fig. 9. (a) Effectiveness of interventions quantified by $P_{[\checkmark^{op_j}|\times^c]}$ (gray curves). The results obtained with the best, θ^B, and worst, θ^W, interventions are shown by green and red curves, respectively. Terms $P^c_\checkmark$, $P^c_\times \cdot P_{[\checkmark^{op_j}|\times^c]}$ and $P^{op_j}_\times$ for (b) $j = \theta^B$ and (c) $j = \theta^W$. (For interpretation of the references to color in this figure legend, the reader is referred to the web version of this article.)

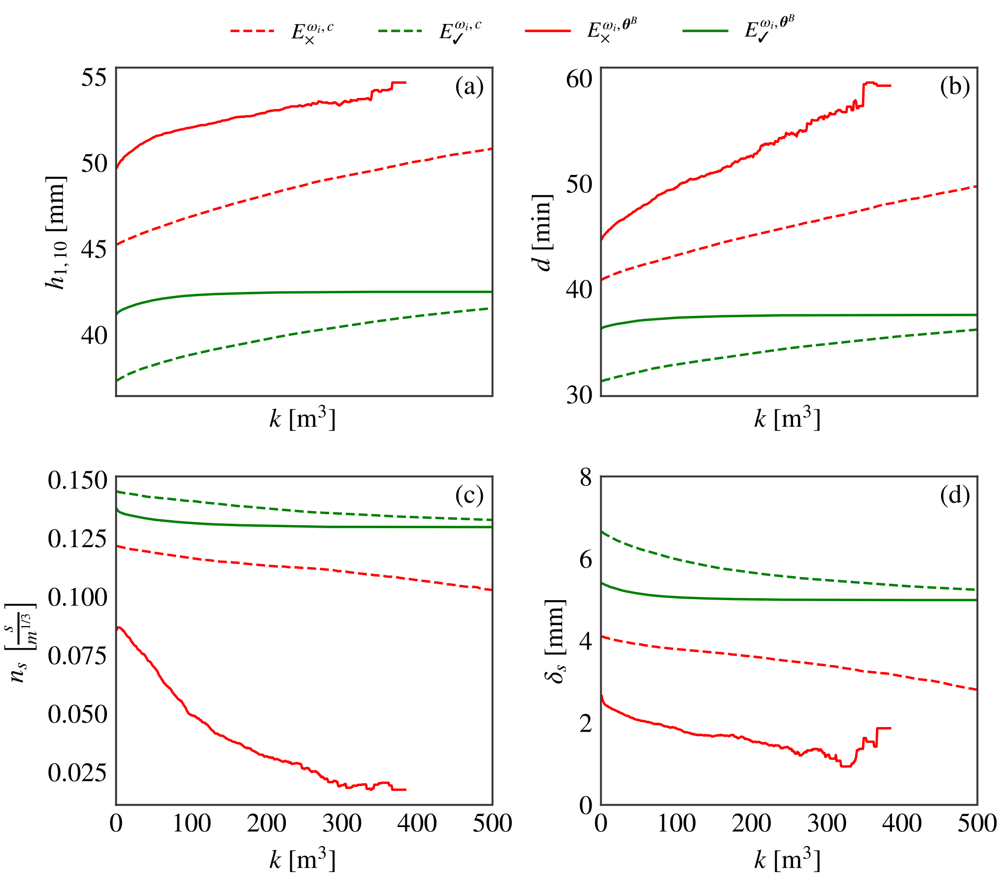

Fig. 10. Expected value of ω_i conditional to system failure $E^{\omega_i,\alpha}_\times$ (red curves) and safety $E^{\omega_i,\alpha}_\checkmark$ (green curves) versus k, for $\alpha = c$ (dashed lines), θ^B (continuous lines). ω_i = (a) $h_{1,10}$; (b) d; (c) n_s; (d) δ_s. (For interpretation of the references to color in this figure legend, the reader is referred to the web version of this article.)

proposed intervention combinations result in a mitigation of the flood volume, compared to the current state scenario, for each realization of $\boldsymbol{\omega}$. This leads to a decrease in the probability of system failure after an intervention, i.e., $P^{op}_\times < P^c_\times$ (see Fig. 8a). At the same time, the difference between $P^c_\times$ and $P^{op}_\times$ decreases as k increases, since an increase in the flood volume deemed acceptable reduces the probability of system failure and the benefit of interventions.

Fig. 8b depicts $\mathrm{AMA}P^{op}_{\theta_i}$, i.e., the mean of $\mathrm{AMA}P_{\theta_i}(\boldsymbol{\omega})$ across the ensemble of $\boldsymbol{\omega}$, versus k. On average (across the ensemble of $\boldsymbol{\omega}$), ϕ has the largest impact on the probability of system failure. Additionally, indices $\mathrm{AMA}P^{op}_{\theta_i}$ exhibit higher values for smaller k thresholds, i.e., an *operational* variable θ_i is more likely to affect the probability of system failure when the threshold k is relatively low, as usually required in urban areas. A similar behavior is observed for the variance of $\mathrm{AMA}P^{op}_{\theta_i}(\boldsymbol{\omega})$ (not shown). These findings can guide stakeholders in prioritizing their attention on ϕ, as it emerges (on average across $\boldsymbol{\omega}$) as the most critical *operational* variable for interventions aimed at mitigating the probability of system failure.

We now proceed to investigate the effectiveness of the envisioned operational interventions in the system. In our study case, the diverse operational interventions are not harmful to the system since: (i) $P_{[\times^{op_j}|\checkmark^c]} = 0$, i.e., if in its current state the system is safe, an intervention will not cause it to fail; or equivalently, (ii) $P_{[\checkmark^{op_j}|\checkmark^c]} = 1$, i.e., if the system is safe in its the current state it will be safe after the interventions. As noted in Fig. 8a, the effectiveness of proposed operational interventions in reducing the probability of system failure diminishes for increasing k, when compared to the current system state. This aspect is further elucidated in Fig. 9a. The latter compares the effectiveness (as expressed in terms of $P_{[\checkmark^{op_j}|\times^c]}$, see Eq. (25)) of diverse operational interventions θ^j (gray curves) versus k. Results obtained with the worst θ^W (red curve) and best θ^B (green curve) combinations of the *operational* variables are highlighted therein. Inspection of Fig. 9a reveals a general decrease in $P_{[\checkmark^{op_j}|\times^c]}$ with k. This is related to the observation that it becomes more challenging to mitigate the system failure (through operational interventions) when extremely large volumes of water are conveyed to the sewer. At the same time, setting $\theta^j = \theta^W$, the effectiveness of the intervention remains approximately constant with k. This finding suggests that, under the least favorable operational settings, interventions could transition from failure to safety only a fixed subset of realizations of $\boldsymbol{\omega}$ (generating reduced volumes of water conveyed to the sewer).

Fig. 9 depicts for (b) θ^B and (c) θ^W: the probability of no failure at the current state, $P^c_{\checkmark}$ (which ensures no failure under operational interventions since $P_{[\checkmark^{op_j}|\checkmark^c]} = 1$ in our case); the probability of failure under the operational intervention, $P^{op_j}_{\times}$; and $P^c_{\times} \cdot P_{[\checkmark^{op_j}|\times^c]}$ which represents the correction through an operational intervention of the system failure (see Eq. (25)) versus k. Note that the evolution of $P^c_{\checkmark}$ with k is identical for both operational conditions. Under θ^B intervention, the term $P^c_{\times} \cdot P_{[\checkmark^{op_j}|\times^c]}$ contributes significantly to reducing the probability of system failure. Conversely, with the intervention θ^W, the impact of $P^c_{\times} \cdot P_{[\checkmark^{op_j}|\times^c]}$ on $P^{op_j}_{\times}$ is marginal, and the reduction of the probability of system failure with k is mainly imputable to the increase of $P^c_{\checkmark}$ (i.e., relaxation of the threshold k that favors the system safety).

Fig. 10 complements the analysis by depicting $E^{\omega_i,\alpha}_{\times}$ (red curves) and $E^{\omega_i,\alpha}_{\checkmark}$ (green curves) with $\alpha = c$ (current state, dashed curves) and $\alpha = \theta^B$ (after the best operational intervention, continuous curves) evaluated based on Eq. (26) as a function of k. These metrics make it possible to determine the mean magnitude of the *non-operational* variables at which the system either fails ($E^{\omega_i,\alpha}_{\times}$) or it is safe ($E^{\omega_i,\alpha}_{\checkmark}$) in the current state and after the intervention θ^B. The number of realizations (across the ensemble $\boldsymbol{\omega}$) where the system fails after the intervention θ^B tends to decrease as k increases. As such, the ensuing estimate of $E^{\omega_i,\theta^B}_{\times}$ becomes noisy and it is then not defined for large threshold values (i.e., no system failure is observed under θ^B for $k > 400$ m^3 in our case). Fig. 10 reveals that: (i) for $\omega_i = (h_{1,10}; d)$, $E^{\omega_i,\theta^B}_{\times} > E^{\omega_i,c}_{\times}$, i.e., when considering θ^B, system failure can be observed during more severe rainfall events than the current system state and (equivalently) $E^{\omega_i,\theta^B}_{\checkmark} > E^{\omega_i,c}_{\checkmark}$, i.e., intervention θ^B allows the system to cope with higher-severity rainfall events than the current system state; and (ii) for $\omega_i = (n_s; \delta_s)$, $E^{\omega_i,\theta^B}_{\times} < E^{\omega_i,c}_{\times}$ and $E^{\omega_i,\theta^B}_{\checkmark} < E^{\omega_i,c}_{\checkmark}$, i.e., under θ^B, system failure occurs in cases where the urban catchment is characterized by reduced surface roughness and/or storage capacity compared to the current system state.

4. Conclusions

We focus on instances of flooding due to the inability of the sewer network in an urban catchment to effectively drain the runoff generated in response to an intense rainfall event. Our study is framed in a stochastic context, encompassing multiple sources of uncertainty. We consider the rainfall event and key catchment characteristics as *non-operational* variables, affected by uncertainty due to our inability to exhaustively characterize them. Additionally, we account for uncertainty related to *operational* variables, which are controllable and modifiable through engineering interventions. We recall that the nature of the variability in the *non-operational* variables differs at a fundamental level from the one associated with *operational* variables. Hence, our approach incorporates both standard and operational Global Sensitivity Analysis (GSA) frameworks. Our study led to the following major conclusions.

- In the current state of the system, uncertainties in the rainfall event characteristics are the main elements impacting the statistical moments and the probability of system failure (i.e., the probability that the flood volume exceeds a threshold). From a practical perspective, this implies that, given the current system state, efforts focused on flood estimation enhancement should prioritize strategies for reducing uncertainty in extreme rainfall predictions.
- When exploring the impact of *operational* variables on flooding, our analyses document that the diameter of sewer conduits is the *operational* variable with the greatest influence (on average across potential scenarios of *non-operational* variables) on diverse statistical moments of the flood volume and the probability of system failure. However, a notable degree of uncertainty is associated with the degree of sensitivity of the flood volume to the diameter of conduits, due to the lack of knowledge about *non-operational* variables. From a practical perspective, these findings emphasize the importance of carefully selecting conduit diameters, taking into account the uncertainty associated with the *non-operational* variables.
- Our stochastic framework allows us to quantify the effectiveness of all proposed interventions. By conducting a GSA on the probability of system failure at the current system state and exploring various operational interventions, the proposed approach allows us to identify the operational setup that offers the highest effectiveness in mitigating flooding events.

The strategy proposed in the present work is general and has the potential to be applied to a variety of studies focused on the sustainability of cities and urban environments when the system behavior is impacted by uncertain *non-operational* and *operational* quantities. The research also contributes to the sustainable development of urban areas by providing a rich understanding of flood risks and assisting in the designing phase of effective flood mitigation strategies.

Potential extensions of this work encompass: (i) including uncertainty in the mathematical models used to describe the physical processes (see Dell'Oca et al., 2023; Dell'Oca, Riva and Guadagnini, 2020); and (ii) integrating multiple target quantities (e.g., floodways, maximum flood velocity) and/or constraints of any nature into the operational variables.

CRediT authorship contribution statement

Leonardo Sandoval: Writing – review & editing, Writing – original draft, Software, Methodology, Data curation. **Aronne Dell'Oca:** Writing – review & editing, Writing – original draft, Supervision, Methodology, Conceptualization. **Monica Riva:** Writing – review & editing, Writing – original draft, Funding acquisition, Formal analysis, Conceptualization.

Declaration of competing interest

The authors declare that they have no known competing financial interests or personal relationships that could have appeared to influence the work reported in this paper.

Acknowledgments

The Authors thank Alberto Guadagnini and acknowledge funding from the European Union's Horizon 2020 research and innovation program under the Marie Skłodowska-Curie program (grant agreement No 872607) in the context of the coordinated research program RECYCLE. M. Riva and A. Dell'Oca acknowledge funding from the National Recovery and Resilience Plan (NRRP), Mission 4 Component 2 Investment 1.4 - Call for tender No. 3138 of December 16, 2021, rectified by Decree n.3175 of December 18, 2021 of Italian Ministry of University and Research funded by the European Union - Next-Generation EU;

Project code CN 00000033, Concession Decree No. 1034 of June 17, 2022 adopted by the Italian Ministry of University and Research, CUP D43C22001250001, Project title "National Biodiversity Future Center - NBFC".

Appendix A. Supplementary data

Supplementary material related to this article can be found online at https://doi.org/10.1016/j.scs.2024.105928.

Data availability

General data about placement and main features of the simulated network elements has been shared in the Supplementary Material. Moreover, codes and notebooks employed for launching simulations, as well as data processing and analysis are available at https://zenodo.org/records/13742805.

References

Arjenaki, M. O., Sanayei, H. R. Z., Heidarzadeh, H., & Mahabadi, N. A. (2021). Modeling and investigating the effect of the LID methods on collection network of urban runoff using the SWMM model (case study: Shahrekord City). *Modeling Earth Systems and Environment*, *7*(1), 1–16. http://dx.doi.org/10.1007/s40808-020-00870-2.

Arnbjerg-Nielsen, K., Willems, P., Olsson, J., Beecham, S., Pathirana, A., Bülow Gregersen, I., et al. (2013). Impacts of climate change on rainfall extremes and urban drainage systems: a review. *Water Science and Technology*, *68*(1), 16–28. http://dx.doi.org/10.2166/wst.2013.251.

Ashley, R., Balmforth, D., Saul, A., & Blanskby, J. (2005). Flooding in the future – predicting climate change, risks and responses in urban areas. *Water Science and Technology*, *52*(5), 265–273. http://dx.doi.org/10.2166/wst.2005.0142.

Azari, B., & Tabesh, M. (2022). Urban storm water drainage system optimization using a sustainability index and LID/BMPs. *Sustainable Cities and Society*, *76*, Article 103500. http://dx.doi.org/10.1016/j.scs.2021.103500.

Bhuiyan, T. R., Er, A. C., Muhamad, N., & Pereira, J. J. (2022). Evaluating the cumulative costs of small-scale flash floods in Kuala Lumpur, Malaysia. *Journal of Hydrology*, *612*, Article 128181. http://dx.doi.org/10.1016/j.jhydrol.2022.128181.

Bodoque, J. M., Esteban-Muñoz, Á., & Ballesteros-Cánovas, J. A. (2023). Overlooking probabilistic mapping renders urban flood risk management inequitable. *Communications Earth & Environment*, *4*(1), 279. http://dx.doi.org/10.1038/s43247-023-00940-0.

Boughton, W. (1989). A review of the USDA SCS curve number method. *Soil Research*, *27*(3), 511–523. http://dx.doi.org/10.1071/SR9890511.

Burlando, P., & Rosso, R. (1996). Scaling and muitiscaling models of depth-duration-frequency curves for storm precipitation. *Journal of Hydrology*, *187*(1–2), 45–64. http://dx.doi.org/10.1016/S0022-1694(96)03086-7.

Chauhan, S., Dongol, R., & Chauhan, R. (2023). Evaluation of economic loss of urban road flooding: A case of Kathmandu Metropolitan City. *Environmental Challenges*, *13*, Article 100773. http://dx.doi.org/10.1016/j.envc.2023.100773.

da Silva, L. B. L., Alencar, M. H., & de Almeida, A. T. (2022). A novel spatiotemporal multi-attribute method for assessing flood risks in urban spaces under climate change and demographic scenarios. *Sustainable Cities and Society*, *76*, Article 103501. http://dx.doi.org/10.1016/j.scs.2021.103501.

D'Ambrosio, R., & Longobardi, A. (2023). Adapting drainage networks to the urban development: An assessment of different integrated approach alternatives for a sustainable flood risk mitigation in Northern Italy. *Sustainable Cities and Society*, *98*, Article 104856. http://dx.doi.org/10.1016/j.scs.2023.104856.

Dell'Oca, A. (2023). Sensitivity Analysis: an operational picture. *Water Resources Research*, *59*(6), Article e2022WR033780. http://dx.doi.org/10.1029/2022WR033780.

Dell'Oca, A., Guadagnini, A., & Riva, M. (2020). Copula density-driven metrics for sensitivity analysis: Theory and application to flow and transport in porous media. *Advances in Water Resources*, *145*, Article 103714. http://dx.doi.org/10.1016/j.advwatres.2020.103714.

Dell'Oca, A., Guadagnini, A., & Riva, M. (2023). Probabilistic assessment of failure of infiltration structures under model and parametric uncertainty. *Journal of Environmental Management*, *344*, Article 118466. http://dx.doi.org/10.1016/j.jenvman.2023.118466.

Dell'Oca, A., Riva, M., & Guadagnini, A. (2017). Moment-based metrics for global sensitivity analysis of hydrological systems. *Hydrology and Earth System Sciences*, *21*(12), 6219–6234. http://dx.doi.org/10.5194/hess-21-6219-2017.

Dell'Oca, A., Riva, M., & Guadagnini, A. (2020). Global sensitivity analysis for multiple interpretive models with uncertain parameters. *Water Resources Research*, *56*(2), Article e2019WR025754. http://dx.doi.org/10.1029/2019WR025754.

Dong, S., Yu, T., Farahmand, H., & Mostafavi, A. (2020). Probabilistic modeling of cascading failure risk in interdependent channel and road networks in urban flooding. *Sustainable Cities and Society*, *62*, Article 102398. http://dx.doi.org/10.1016/j.scs.2020.102398.

Forsee, W. J., & Ahmad, S. (2011). Evaluating urban storm-water infrastructure design in response to projected climate change. *Journal of Hydrologic Engineering*, *16*(11), 865–873. http://dx.doi.org/10.1061/(ASCE)HE.1943-5584.0000383.

Gray, L. C., Zhao, L., & Stillwell, A. S. (2023). Impacts of climate change on global total and urban runoff. *Journal of Hydrology*, *620*, Article 129352. http://dx.doi.org/10.1016/j.jhydrol.2023.129352.

Haghighatafshar, S., Becker, P., Moddemeyer, S., Persson, A., Sörensen, J., Aspegren, H., et al. (2020). Paradigm shift in engineering of pluvial floods: From historical recurrence intervals to risk-based design for an uncertain future. *Sustainable Cities and Society*, *61*, Article 102317. http://dx.doi.org/10.1016/j.scs.2020.102317.

Hammond, M., Chen, A., Djordjević, S., Butler, D., & Mark, O. (2015). Urban flood impact assessment: A state-of-the-art review. *Urban Water Journal*, *12*(1), 14–29. http://dx.doi.org/10.1080/1573062X.2013.857421.

Hesarkazzazi, S., Hajibabaei, M., Bakhshipour, A. E., Dittmer, U., Haghighi, A., & Sitzenfrei, R. (2022). Generation of optimal (de)centralized layouts for urban drainage systems: A graph-theory-based combinatorial multi-objective optimization framework. *Sustainable Cities and Society*, *81*, Article 103827. http://dx.doi.org/10.1016/j.scs.2022.103827.

Hu, C., Xia, J., She, D., Song, Z., Zhang, Y., & Hong, S. (2021). A new urban hydrological model considering various land covers for flood simulation. *Journal of Hydrology*, *603*, Article 126833. http://dx.doi.org/10.1016/j.jhydrol.2021.126833.

Huong, H. T. L., & Pathirana, A. (2013). Urbanization and climate change impacts on future urban flooding in Can Tho city, Vietnam. *Hydrology and Earth System Sciences*, *17*(1), 379–394. http://dx.doi.org/10.5194/hess-17-379-2013.

Iradukunda, P., Mwanaumo, E. M., & Kabika, J. (2023). A review of integrated multicriteria decision support analysis in the climate resilient infrastructure development. *Environmental and Sustainability Indicators*, *20*, Article 100312. http://dx.doi.org/10.1016/j.indic.2023.100312.

Jato-Espino, D., Toro-Huertas, E. I., & Güereca, L. P. (2022). Lifecycle sustainability assessment for the comparison of traditional and sustainable drainage systems. *Science of the Total Environment*, *817*, Article 152959. http://dx.doi.org/10.1016/j.scitotenv.2022.152959.

Ju, X., Li, W., Li, J., He, L., Mao, J., & Han, L. (2023). Future climate change and urban growth together affect surface runoff in a large-scale urban agglomeration. *Sustainable Cities and Society*, *99*, Article 104970. http://dx.doi.org/10.1016/j.scs.2023.104970.

Jung, I.-W., Chang, H., & Moradkhani, H. (2011). Quantifying uncertainty in urban flooding analysis considering hydro-climatic projection and urban development effects. *Hydrology and Earth System Sciences*, *15*(2), 617–633. http://dx.doi.org/10.5194/hess-15-617-2011.

KC, S., Shrestha, S., Ninsawat, S., & Chonwattana, S. (2021). Predicting flood events in Kathmandu Metropolitan City under climate change and urbanisation. *Journal of Environmental Management*, *281*, Article 111894. http://dx.doi.org/10.1016/j.jenvman.2020.111894.

Kidd, C. (1978). *Rainfall-runoff processes over urban surfaces*: *Technical Report*, Institute of Hydrology of United Kingdom.

la Cecilia, D., Porta, G. M., Tang, F. H., Riva, M., & Maggi, F. (2020). Probabilistic indicators for soil and groundwater contamination risk assessment. *Ecological Indicators*, *115*, Article 106424. http://dx.doi.org/10.1016/j.ecolind.2020.106424.

Li, X., Zhou, Y., Hejazi, M., Wise, M., Vernon, C., Iyer, G., et al. (2021). Global urban growth between 1870 and 2100 from integrated high resolution mapped data and urban dynamic modeling. *Communications Earth & Environment*, *2*(1), 201. http://dx.doi.org/10.1038/s43247-021-00273-w.

Liu, W., Feng, Q., Engel, B. A., Yu, T., Zhang, X., & Qian, Y. (2023). A probabilistic assessment of urban flood risk and impacts of future climate change. *Journal of Hydrology*, *618*, Article 129267. http://dx.doi.org/10.1016/j.jhydrol.2023.129267.

Liu, X., Huang, Y., Xu, X., Li, X., Li, X., Ciais, P., et al. (2020). High-spatiotemporal-resolution mapping of global urban change from 1985 to 2015. *Nature Sustainability*, *3*(7), 564–570. http://dx.doi.org/10.1038/s41893-020-0521-x.

de Macedo, M. B., Mendiondo, E. M., Razzolini, M. T. P., Goel, N. K., Arya, D. S., Kurian, M., et al. (2023). Multi-stage resilience analysis of the nexus flood-sanitation-public health in urban environments: a theoretical framework. *Urban Water Journal*, *20*(10), 1713–1730. http://dx.doi.org/10.1080/1573062X.2022.2047737.

Mahaut, V., & Andrieu, H. (2019). Relative influence of urban-development strategies and water management on mixed (separated and combined) sewer overflows in the context of climate change and population growth: A case study in Nantes. *Sustainable Cities and Society*, *44*, 171–182. http://dx.doi.org/10.1016/j.scs.2018.09.012.

Mahmoud, S. H., & Gan, T. Y. (2018). Urbanization and climate change implications in flood risk management: Developing an efficient decision support system for flood susceptibility mapping. *Science of the Total Environment*, *636*, 152–167. http://dx.doi.org/10.1016/j.scitotenv.2018.04.282.

de Michele, C., Rosso, R., & Rulli, M. C. (2005). *Il regime delle precipitazioni intense sul territorio della Lombardia*: *Technical Report*, Politecnico di Milano.

Miller, J. D., & Hutchins, M. (2017). The impacts of urbanisation and climate change on urban flooding and urban water quality: A review of the evidence concerning the United Kingdom. *Journal of Hydrology: Regional Studies*, *12*, 345–362. http://dx.doi.org/10.1016/j.ejrh.2017.06.006.

Mobini, S., Pirzamanbein, B., Berndtsson, R., & Larsson, R. (2022). Urban flood damage claim analyses for improved flood damage assessment. *International Journal of Disaster Risk Reduction*, *77*, Article 103099. http://dx.doi.org/10.1016/j.ijdrr.2022.103099.

Mohammed, M. H., Zwain, H. M., & Hassan, W. H. (2021). Modeling the impacts of climate change and flooding on sanitary sewage system using SWMM simulation: A case study. *Results in Engineering*, *12*, Article 100307. http://dx.doi.org/10.1016/j.rineng.2021.100307.

O'Donnell, E. C., & Thorne, C. R. (2020). Drivers of future urban flood risk. *Philosophical Transactions of the Royal Society of London A (Mathematical and Physical Sciences)*, *378*(2168), Article 20190216. http://dx.doi.org/10.1098/rsta.2019.0216.

Pianosi, F., Beven, K., Freer, J., Hall, J. W., Rougier, J., Stephenson, D. B., et al. (2016). Sensitivity analysis of environmental models: A systematic review with practical workflow. *Environmental Modelling & Software*, *79*, 214–232. http://dx.doi.org/10.1016/j.envsoft.2016.02.008.

Pińskwar, I., Choryński, A., & Graczyk, D. (2023). Risk of flash floods in urban and rural municipalities triggered by intense precipitation in Wielkopolska of Poland. *International Journal of Disaster Risk Science*, *14*(3), 440–457. http://dx.doi.org/10.1007/s13753-023-00493-y.

Piyumi, M., Abenayake, C., Jayasinghe, A., & Wijegunarathna, E. (2021). Urban flood modeling application: Assess the effectiveness of building regulation in coping with urban flooding under precipitation uncertainty. *Sustainable Cities and Society*, *75*, Article 103294. http://dx.doi.org/10.1016/j.scs.2021.103294.

Pour, S. H., Wahab, A. K. A., Shahid, S., Asaduzzaman, M., & Dewan, A. (2020). Low impact development techniques to mitigate the impacts of climate-change-induced urban floods: Current trends, issues and challenges. *Sustainable Cities and Society*, *62*, Article 102373. http://dx.doi.org/10.1016/j.scs.2020.102373.

Razavi, S., Jakeman, A., Saltelli, A., Prieur, C., Iooss, B., Borgonovo, E., et al. (2021). The Future of Sensitivity Analysis: An essential discipline for systems modeling and policy support. *Environmental Modelling & Software*, *137*, Article 104954. http://dx.doi.org/10.1016/j.envsoft.2020.104954.

Rossman, L. A. (2010). *Storm water management model user's manual, version 5.0*. National Risk Management Research Laboratory, Office of Research and Development.

Rossman, L. A. (2017). Storm water management model reference manual volume II - Hydraulics.

Satterthwaite, D. (2008). Climate change and urbanization: Effects and implications for urban governance. In *United nations expert group meeting on population distribution, urbanization, internal migration and development* (pp. 309–334). New York: DESA.

Semadeni-Davies, A., Hernebring, C., Svensson, G., & Gustafsson, L.-G. (2008). The impacts of climate change and urbanisation on drainage in Helsingborg, Sweden: Combined sewer system. *Journal of Hydrology*, *350*(1–2), 100–113. http://dx.doi.org/10.1016/j.jhydrol.2007.05.028.

Suresh, A., Pekkat, S., & Subbiah, S. (2023). Quantifying the efficacy of Low Impact Developments (LIDs) for flood reduction in micro-urban watersheds incorporating climate change. *Sustainable Cities and Society*, *95*, Article 104601. http://dx.doi.org/10.1016/j.scs.2023.104601.

Tavakol-Davani, H., Goharian, E., Hansen, C. H., Tavakol-Davani, H., Apul, D., & Burian, S. J. (2016). How does climate change affect combined sewer overflow in a system benefiting from rainwater harvesting systems? *Sustainable Cities and Society*, *27*, 430–438. http://dx.doi.org/10.1016/j.scs.2016.07.003.

Tellman, B., Sullivan, J. A., Kuhn, C., Kettner, A. J., Doyle, C. S., Brakenridge, G. R., et al. (2021). Satellite imaging reveals increased proportion of population exposed to floods. *Nature*, *596*(7870), 80–86. http://dx.doi.org/10.1038/s41586-021-03695-w.

ten Veldhuis, J. (2011). How the choice of flood damage metrics influences urban flood risk assessment. *Journal of Flood Risk Management*, *4*(4), 281–287. http://dx.doi.org/10.1111/j.1753-318X.2011.01112.x.

Viessman, W., & Lewis, G. L. (2003). *Introduction to hydrology*. Prentice Hall.

Wang, M., Liu, M., Zhang, D., Zhang, Y., Su, J., Zhou, S., et al. (2023). Assessing hydrological performance for optimized integrated grey-green infrastructure in response to climate change based on shared socio-economic pathways. *Sustainable Cities and Society*, *91*, Article 104436. http://dx.doi.org/10.1016/j.scs.2023.104436.

Wang, Y., Zhang, C., Chen, A. S., Wang, G., & Fu, G. (2023). Exploring the relationship between urban flood risk and resilience at a high-resolution grid cell scale. *Science of the Total Environment*, *893*, Article 164852. http://dx.doi.org/10.1016/j.scitotenv.2023.164852.

Xu, H., Zhong, T., Chen, Y., & Zhang, J. (2023). How to simulate future scenarios of urban stormwater management? A novel framework coupling climate change, urbanization, and green stormwater infrastructure development. *Science of the Total Environment*, *874*, Article 162399. http://dx.doi.org/10.1016/j.scitotenv.2023.162399.

Yin, J., Gentine, P., Zhou, S., Sullivan, S. C., Wang, R., Zhang, Y., et al. (2018). Large increase in global storm runoff extremes driven by climate and anthropogenic changes. *Nature Communications*, *9*(1), 4389. http://dx.doi.org/10.1038/s41467-018-06765-2.

Yu, D., & Coulthard, T. J. (2015). Evaluating the importance of catchment hydrological parameters for urban surface water flood modelling using a simple hydro-inundation model. *Journal of Hydrology*, *524*, 385–400. http://dx.doi.org/10.1016/j.jhydrol.2015.02.040.

Zeighami, F., Sandoval, L., Guadagnini, A., & Di Federico, V. (2023). Uncertainty quantification and global sensitivity analysis of seismic metabarriers. *Engineering Structures*, *277*, Article 115415. http://dx.doi.org/10.1016/j.engstruct.2022.115415.

Zhao, H., Gu, T., Tang, J., Gong, Z., & Zhao, P. (2023). Urban flood risk differentiation under land use scenario simulation. *iScience*, *26*(4), Article 106479. http://dx.doi.org/10.1016/j.isci.2023.106479.